

iLogDemons: A Demons-Based Registration Algorithm for Tracking Incompressible Elastic Biological Tissues

Tommaso Mansi · Xavier Pennec · Maxime Sermesant · Hervé Delingette · Nicholas Ayache

Received: date / Accepted: date

Abstract Tracking soft tissues in medical images using non-linear image registration algorithms requires methods that are fast and that provide spatial transformations consistent with the biological characteristics of the tissues. LogDemons algorithm is a fast non-linear registration method that computes diffeomorphic transformations parameterised by a stationary velocity field. Despite its computational efficiency, its use for tissue tracking has been limited because of its *ad-hoc* Gaussian regularisation, which hampers the implementation of more biological regularisations. In this work, we improve logDemons by integrating elasticity and incompressibility for soft-tissue tracking. To that end, a mathematical justification of demons Gaussian regularisation is proposed. Building on this result, we replace the Gaussian smoothing by an efficient elastic-like regulariser based on isotropic differential quadratic forms of vector fields. The registration energy functional is finally minimised under the divergence-free constraint to get incompressible deformations. As the elastic regulariser and the constraint are linear, the method remains computationally tractable and easy to implement. Tests on synthetic incompressible deformations showed that our approach outperforms the original logDemons in terms of elastic incompressible deformation recovery without reducing image matching accuracy. As an application, we applied the proposed algorithm to estimate 3D myocardium strain on clinical cine MRI of two adult patients. Results showed that incompressibility constraint better estimate the cardiac motion when compared to the ground truth provided by 3D tagged MRI.

Keywords Demons Algorithm · Gaussian Smoothing · Elastic-like Regularisation · Incompressible Registration · Stationary Velocity Field · Divergence-Free Velocity

1 Introduction

Tissue tracking in sequences of medical images is an important task in many clinical applications, either for disease diagnosis or therapy guidance. However there is no easy way to achieve it, even interactively. A standard approach is to use non-linear image registration to estimate dense spatial transformations between images. For instance, cardiac motion is estimated by non-linearly co-registering the frames of the cardiac sequence, yielding a dense displacement field that quantifies myocardium motion (Bistoquet et al, 2008).

In practice, non-linear image registration is performed by minimising a dissimilarity criterion between the images to register up to a regularisation term that ensures smooth transformations by modelling prior knowledge about the spatial transformations. For clinical applications, the impenetrability of matter must be ensured, i.e. transformations must be smooth one-to-one mappings. In addition, the model of transformations must be consistent with the properties of the tissue to track, such as elasticity and incompressibility. This is all the more important if the estimated deformations are used to analyse anatomical changes between different time points (Ashburner et al, 1998). However, adding these constraints to image registration algorithms are often achieved at the price of computational complexity. In this paper, an efficient non-linear registration algorithm based on the fast demons approach is proposed for tracking elastic and incompressible soft tissues.

T. Mansi, X. Pennec, M. Sermesant, H. Delingette and N. Ayache
2004 Route des Lucioles - BP 93, 06902 Sophia Antipolis, France
Tel.: +33-4-92-38-71-56
Fax: +33-4-92-38-76-69
E-mail: Tommaso.Mansi@sophia.inria.fr

1.1 Diffeomorphic Non-Linear Image Registration

With the recent advances in computational anatomy, mathematical frameworks based on diffeomorphic deformations have been developed to estimate one-to-one differentiable mappings between the images to register. The underlying idea is to parameterise the transformations by velocity fields according to the Lagrange transport equation (Arnold, 1989). When the velocity fields vary over time, large diffeomorphic deformations can be estimated using the Large Deformation Diffeomorphic Metric Mappings (LDDMM) (Miller et al, 2002; Beg et al, 2005). However, complex partial differential equations must be solved to integrate the velocity field over time along a geodesic path, resulting in high computational cost. To tackle this limitation, recent works relied on *stationary* velocity fields, which are integrated very efficiently through exponential maps (Arsigny et al, 2006a; Bossa et al, 2007; Hernandez et al, 2009).

Among the methods based on stationary velocities, *log-Demons* (Vercauteren et al, 2008) is a very efficient non-linear registration algorithm based on the demons alternate optimisation (Thirion, 1998). Two images are registered by alternating an optimisation step, which updates the stationary velocity field in a voxel-wise manner, and a Gaussian smoothing step, which models a diffusion motion. LogDemons algorithm is appealing as it ensures diffeomorphic mappings, it enables working on velocities and transformations simultaneously and its complexity is linear in the number of voxel. However, the diffusion model may not be appropriate for tracking biological tissues as it has no physical meaning. If mathematical justifications of demons optimisation step have been provided (Cachier et al, 2003; Vercauteren et al, 2009), theoretical foundations of the Gaussian regularisation still has to be consolidated (Pennec et al, 1999; Modersitzki, 2004; Cahill et al, 2009). This paper presents a mathematical justification of demons Gaussian regularisation which enables estimating *elastic* and *incompressible* deformations.

1.2 Elastic Non-Linear Image Registration

First introduced by Broit (1981), elastic registration algorithms consist in regularising the transformations by using the linear elasticity equation, also known as Lamé equation. Although computationally efficient, these regularisers are suitable for small displacements only and can yield discontinuities in the derivatives of the regularised deformations (Modersitzki, 2004). Techniques based on smooth elastic-body splines have been developed (Rueckert et al, 1999; Sorzano et al, 2005). Yet, they are computationally demanding and diffeomorphic mappings are ensured through ad-hoc penalisation of the registration energy (Rueckert et al, 2006; DeCraene et al, 2009), which makes the computation of the inverse transformation critical. Cachier and Ayache (2004)

demonstrated that the linear Lamé equation is actually a specific first order isotropic quadratic form (IDQF) of the transformation. High order IDQF can be designed, resulting in elastic-like regularisation of any order of smoothness. Cachier and Ayache (2004) also conjectured a separable elastic-like vector filter that behaves like an IDQF of infinite order. This filter has been used in demons algorithms in place of the Gaussian kernel (Cachier and Ayache, 2004; Mansi et al, 2009). However, its link with IDQF energies is not clear. In this paper we investigate how this filter relates to IDQF to rigorously integrate it in logDemons regularisation energy.

1.3 Incompressible Non-Linear Image Registration

Incompressible deformations cannot be recovered with elastic regularisers alone, explicit constraints must be added. A transformation is volume-preserving if its Jacobian determinant equals one. This constraint is non-linear and requires *ad-hoc* numerical schemes that are computationally demanding (Rohlfing et al, 2003; Haber and Modersitzki, 2004). Bistoquet et al (2008) proposed to use the linear approximation of that constraint, i.e. the divergence of the displacements is null. However, volume drifts appear when deformations become large, which the authors controlled by penalising the energy functional.

When estimating fluid motion, incompressibility is satisfied if the velocity of the fluid is divergence-free. Building up on this observation, countless optical flow techniques (Horn and Schunck, 1981) based on the continuity equation and the divergence-free constraint have been developed to estimate incompressible fluid motion from 3D images (see (Heitz et al, 2009) and reference therein). Song and Leahy (1991) and Gorce et al (1997) applied this approach to estimate 3D cardiac velocity from cine CT images. Cuzol et al (2007) combined the optical flow algorithm with the Helmholtz decomposition to estimate 2D fluid motions parameterised by divergence-free and curl-free parameter maps. Saddi et al (2007) constrained a fluid registration algorithm to be incompressible by projecting the update velocities onto the space of divergence-free vector field using Helmholtz decomposition. All these techniques showed satisfying results and demonstrated that incompressibility constraints can improve the estimation of incompressible fluid motion. However, the fluid model may not be suitable for tracking elastic biological tissues: the incompressibility condition on the transformation is usually preferred for biological applications.

Interestingly, one can demonstrate that diffeomorphic transformations parameterised by divergence-free velocity fields through the transport equation are incompressible (Evans, 1998). Hinkle et al (2009) for instance used this property to guide image reconstruction of incompressible organ with

LDDMM and divergence-free time varying velocity fields. This paper extends our previous approach (Mansi et al, 2009), we rely on divergence-free stationary velocity fields to integrate the incompressibility constraint in the logDemons algorithm.

1.4 Model-Based Non-Linear Image Registration

For tracking biological tissues, some works proposed to guide non-linear registration algorithms with biomechanical models that simulate the tissue to track. These approaches have been successfully applied in cardiac motion estimation (Papademetris et al, 2000; Sinusas et al, 2001; Veress et al, 2005; Phatak et al, 2009; Sundar et al, 2009a) and brain shift estimation (Ferrant et al, 2001; Clatz et al, 2005). However, the underlying models often rely on physical parameters that are difficult to determine for a given patient. Besides, such models may not apply anymore in diseases. Finally, they all require meshing the space domain in order to solve complex partial differential equations. For all these reasons we prefer here a purely image-driven algorithm.

1.5 Aim and Paper Organisation

This paper proposes a consistent and efficient framework for elastic incompressible non-linear registration based on logDemons algorithm. Contrary to our previous work (Mansi et al, 2009), this approach operates entirely in the log-domain. The constraint is strong and applied directly in the demons minimisation space. After a brief introduction to the log-Demons algorithm (Section 2), we propose a mathematical justification of demons Gaussian regularisation that enables adapting the algorithm to other transformation models (Section 3). We then replace that regulariser with multi-order IDQF whose minimiser is exactly computed with Cachier and Ayache (2004) elastic-like vector filter. Finally, strong incompressibility is ensured by constraining the stationary velocity fields that parameterise the transformations to be divergence-free (Section 4). Our method, hereafter termed *iLogDemons*, is mathematically consistent as all its elements and parameters are controlled. The proposed demons framework results in the following advantages with respect to previous techniques: 1) the elastic regulariser and the incompressibility constraint are linear, yielding low computational overhead, 2) they are rigorously integrated in the demons energy functional, yielding closed form minimisers that can be easily enabled/disabled by the user and applied to sub-domains of the images, and 3) incompressibility constraint is strong: no volume drifts appear. Section 5 reports results on synthetic datasets with known ground truth. As a clinical application, we employed iLogDemons to estimate myocardium motion and strain on clinical cine MR images of

the heart of two adult patients with heart failure. In both experiments, iLogDemons improved the recovery of incompressible transformations compared with the original log-Demons.

2 Background: Log-Domain Diffeomorphic Demons

Proposed by (Vercauteren et al, 2008), log-domain diffeomorphic demons, hereafter termed *logDemons*, is an efficient non-linear registration algorithm based on demons approach (Thirion, 1998). Given a reference image R and a template image T , logDemons estimates a dense spatial transformation ϕ that best aligns T to R . This is achieved by alternating an *optimisation step*, which updates the transformation in a voxel-wise manner, and a *regularisation step*, which traditionally consists in Gaussian smoothing. Cachier et al (2003) justified the demons algorithm by the alternate minimisation of the energy functional:

$$\mathcal{E}(\phi, \phi_c) = \frac{1}{\sigma_i^2} \|R - T \circ \phi_c\|_{L_2}^2 + \frac{1}{\sigma_x^2} \text{dist}(\phi_c, \phi) + \frac{1}{\sigma_d^2} \|\nabla \phi\|^2 \quad (1)$$

In this equation, ϕ is the dense spatial transformation to estimate and ϕ_c is an intermediate transformation, called *correspondences*, that matches the two images without considering the regularity of the transformation. The first term of (1) is the similarity criterion or data-term. It measures how R and $T \circ \phi_c$ are similar. σ_i^2 relates to the noise in the images. The last term of (1) is the regulariser whose strength is controlled by σ_d^2 . It ensures the spatial smoothness of the transformation ϕ , here by penalising large gradients, and models prior knowledge about the transformation to recover. The second term of (1) couples the correspondences ϕ_c with the smooth transformation ϕ . It unifies in a common mathematical framework the optimisation step, which amounts to minimising $\mathcal{E}(\phi, \phi_c)$ with respect to ϕ_c , and the regularisation step, which consists in minimising $\mathcal{E}(\phi, \phi_c)$ with respect to ϕ .

In logDemons, the registration energy (1) is adapted to estimate spatial transformations that are parameterised by stationary velocity fields \mathbf{v} through the exponential map $\phi = \exp(\mathbf{v})$. Such transformations belong to the subspace of diffeomorphisms \mathbb{G} generated by the one-parameter subgroups of diffeomorphisms. The tangent space of velocities V is the *log-domain*. As \mathbf{v} is stationary, the exponential map $\exp(\mathbf{v})$ is efficiently computed using a “scaling-and-squaring” algorithm (Arsigny et al, 2006a) (Appendix A). Alternatively, ϕ can be defined as the solution of the Lagrange transport equation: $\partial \phi(\mathbf{x}, t) / \partial t = \mathbf{v}(\phi(\mathbf{x}, t))$, $\phi(\mathbf{x}, 0) = \mathbf{x}$. With $\phi = \exp(\mathbf{v})$ and $\phi_c = \exp(\mathbf{v}_c)$, logDemons energy writes in the

log-domain:

$$\begin{aligned} \mathcal{E}(\mathbf{v}, \mathbf{v}_c) = & \frac{1}{\sigma_i^2} \|R - T \circ \exp(\mathbf{v}_c)\|_{L_2}^2 + \\ & \frac{1}{\sigma_x^2} \|\log(\exp(-\mathbf{v}) \circ \exp(\mathbf{v}_c))\|_{L_2}^2 + \frac{1}{\sigma_d^2} \|\nabla \mathbf{v}\|^2 \end{aligned} \quad (2)$$

During the optimisation step, we minimise $\mathcal{E}(\mathbf{v}, \mathbf{v}_c)$ with respect to \mathbf{v}_c . The correspondence field ϕ_c is modelled with the diffeomorphic update rule $\phi_c \leftarrow \phi \circ \exp(\delta \mathbf{v})$, where ϕ is the current estimate of the transformation to recover and $\delta \mathbf{v}$ is an unknown small update velocity field, the so-called demons force. Using Gauss-Newton algorithm and an efficient second-order minimisation (ESM) scheme yields:

$$\delta \mathbf{v}(\mathbf{x}) = -\frac{R(\mathbf{x}) - T \circ \phi(\mathbf{x})}{\|J(\mathbf{x})\|^2 + \sigma_i^2 / \sigma_x^2} J(\mathbf{x}) \quad (3)$$

where $J(\mathbf{x})$ is the symmetric gradient $J(\mathbf{x}) = (\nabla R(\mathbf{x}) + \nabla(T \circ \phi)(\mathbf{x})) / 2$. In virtue of the diffeomorphic update rule $\phi_c = \phi \circ \exp(\delta \mathbf{v}) = \exp(\mathbf{v}) \circ \exp(\delta \mathbf{v})$, we can apply Baker-Campbell-Hausdorff (BCH) formula to estimate the correspondence velocity \mathbf{v}_c without computing the logarithm of the updated correspondences ϕ_c . Indeed, BCH formula gives an approximation of the velocity field $\mathbf{v}_c = Z(\mathbf{v}, \delta \mathbf{v})$ such that $\exp(\mathbf{v}_c) = \exp(\mathbf{v}) \circ \exp(\delta \mathbf{v})$. As shown in (Vercauteren et al, 2008), the first order approximation is sufficient for image registration purposes. We thus have:

$$\begin{aligned} \mathbf{v}_c &= Z(\mathbf{v}, \delta \mathbf{v}) \\ &= \mathbf{v} + \delta \mathbf{v} + 1/2[\mathbf{v}, \delta \mathbf{v}] + 1/12[\mathbf{v}, [\mathbf{v}, \delta \mathbf{v}]] + O(\|\delta \mathbf{v}\|^2) \end{aligned} \quad (4)$$

In the previous equation, the Lie bracket $[\cdot, \cdot]$ is defined by $[\mathbf{v}, \delta \mathbf{v}] = (\nabla \mathbf{v}) \delta \mathbf{v} - (\nabla \delta \mathbf{v}) \mathbf{v}$. Although it is not clear whether theoretically the space \mathbb{G} is a BCH-Lie group (Glockner, 2006), BCH composition of diffeomorphisms of \mathbb{G} has experimentally shown promising results in terms of image registration and statistics on diffeomorphisms (Bossa et al, 2007; Vercauteren et al, 2008).

Once \mathbf{v}_c is calculated, (2) is minimised with respect to \mathbf{v} . This step is performed by smoothing \mathbf{v}_c with a Gaussian kernel G_σ . Next section investigates how this smoothing relates to $\mathcal{E}(\mathbf{v}, \mathbf{v}_c)$. The main steps of the logDemons algorithm are reported in the pseudo-code (Algorithm 1).

About LogDemons Parameters LogDemons is controlled by four parameters: the image noise σ_i^2 , the uncertainty on the correspondences σ_x^2 and the regularisation strengths σ_f^2 and σ^2 . The noise in the images is estimated at every voxel by $\sigma_i^2(\mathbf{x}) = |R(\mathbf{x}) - T \circ \phi(\mathbf{x})|^2$ (Cachier et al, 1999; Vercauteren et al, 2009). As in Thirion demons, such an estimator normalises $\delta \mathbf{v}$ to prevent too strong updates that would hamper the stability of the algorithm. In particular, building on (Cachier et al, 1999), Vercauteren et al (2009) demonstrated that the maximum amplitude of the update velocity $\delta \mathbf{v}$ is

Algorithm 1 LogDemons Registration

Require: Stationary velocity field \mathbf{v}^0 . {Usually $\mathbf{v}^0 = \mathbf{0}$, i.e. $\phi^0 = \text{Id}$ }.

- 1: **loop** {over n until convergence}
- 2: Compute the update velocity: $\delta \mathbf{v}^n$ given \mathbf{v}^{n-1} (3).
- 3: Fluid-like registration: $\mathbf{v}^n \leftarrow G_{\sigma_f} \star \delta \mathbf{v}^n$, G_{σ_f} is a Gaussian kernel.
- 4: Update the velocity field: $\mathbf{v}^n \leftarrow Z(\mathbf{v}^{n-1}, \delta \mathbf{v}^n)$ (4).
- 5: Diffusion-like registration: $\mathbf{v}^n \leftarrow G_\sigma \star \mathbf{v}^n$, G_σ is a Gaussian kernel.
- 6: **end loop**
- 7: **return** \mathbf{v} , $\phi = \exp(\mathbf{v})$ and $\phi^{-1} = \exp(-\mathbf{v})$.

upper bounded by $\sigma_x/2$. However, more global noise estimators fail to upper bound the update velocities, which can become large and ultimately yield non diffeomorphic transformations. This behaviour was confirmed experimentally using Gaussian based noise estimated. σ_f^2 controls the strength of the fluid-like regularisation. In practice, $\sigma_f^2 = 0.5$ is recommended. Finally, σ^2 controls the strength of the regularisation, as we shall discuss in the next section. It has to be stressed that here, the three parameters σ_x^2 , σ_f^2 and σ^2 are explicitly decoupled as in (Cachier et al, 2003; Vercauteren et al, 2008) in contrast to other formulations of demons where σ_x^2 is implicit.

3 Insights on LogDemons Regularisation: From Diffusion to Elastic-Like Regularisation

3.1 Insights on LogDemons Gaussian Regularisation

A consistent mathematical formulation of logDemons regularisation is required to adapt the algorithm to other transformation models. In scale-space theory, Nielsen et al (1994) demonstrated that the Gaussian smoothing is the solution to the Tikhonov estimation problem with equal weighting of the spatial derivatives in the Taylor series sense. We thus replace the first-order logDemons regulariser $\|\nabla \mathbf{v}\|^2 / \sigma_d^2$ by the infinite sum Tikhonov regulariser defined by:

$$\mathcal{R}_{dif}(\mathbf{v}) = \int_{\Omega} \sum_{k=1}^{+\infty} \frac{\partial_{i_1 \dots i_k} \mathbf{v}_{i_{k+1}} \partial_{i_1 \dots i_k} \mathbf{v}_{i_{k+1}}}{\sigma_x^2 \sigma_d^{2k} k!} \quad (5)$$

In this equation, Ω is the image domain and $\partial_{i_k \dots i_l}$ denotes the composition of spatial derivatives $\partial_{i_k} \dots \partial_{i_l}$. A simplified Einstein notation convention is used: Indices that are repeated twice in a product are summed all over their range (e.g. $\mathbf{v}_i \mathbf{v}_i = \mathbf{v}_1^2 + \mathbf{v}_2^2 + \mathbf{v}_3^2$ if $\mathbf{v} : \mathbb{R}^3 \rightarrow \mathbb{R}^3$). \mathcal{R}_{dif} has been divided by σ_x^2 to simplify calculations and the regularisation weight σ_d^2 is function of the derivative orders to preserve the shape of the impulse response related to the regulariser (Nielsen et al, 1994). Minimising the registration energy (2), modified using (5), with respect to \mathbf{v} amounts to minimising

the regularisation energy:

$$\begin{aligned}\mathcal{E}_{reg}(\mathbf{v}) &= \frac{1}{\sigma_x^2} \|\log(\exp(-\mathbf{v}) \circ \exp(\mathbf{v}_c))\|_{L_2}^2 \\ &+ \int_{\Omega} \sum_{k=1}^{+\infty} \frac{\partial_{i_1..i_k} \mathbf{v}_{i_{k+1}} \partial_{i_1..i_k} \mathbf{v}_{i_{k+1}}}{\sigma_x^2 \sigma_d^{2k} k!}\end{aligned}\quad (6)$$

By linearising the first term using the zeroth order approximation of BCH formula (4), $\log(\exp(-\mathbf{v}) \circ \exp(\mathbf{v}_c)) \approx \mathbf{v}_c - \mathbf{v}$, (6) becomes a Tikhonov estimation problem:

$$\mathcal{E}_{reg}(\mathbf{v}) = \frac{1}{\sigma_x^2} \|\mathbf{v}_c - \mathbf{v}\|_{L_2}^2 + \int_{\Omega} \sum_{k=1}^{+\infty} \frac{\partial_{i_1..i_k} \mathbf{v}_{i_{k+1}} \partial_{i_1..i_k} \mathbf{v}_{i_{k+1}}}{\sigma_x^2 \sigma_d^{2k} k!} \quad (7)$$

It follows from the optimal condition $\partial_{\mathbf{v}} \mathcal{E}_{reg}(\mathbf{v}) = 0$:

$$\mathbf{v} + \sum_{k=1}^{+\infty} \frac{(-1)^k}{\sigma_d^{2k}} \frac{\Delta^k \mathbf{v}}{k!} = \mathbf{v}_c$$

where Δ is the Laplacian operator. We solve this equation in the Fourier domain. Let $\hat{\mathbf{v}}(\mathbf{w}) = \mathfrak{F}(\mathbf{v}(\mathbf{x}))$ be the Fourier transform of the velocity field $\mathbf{v}(\mathbf{x})$, \mathbf{w} is the frequency variable. We have:

$$\sum_{k=0}^{\infty} \frac{(\mathbf{w}^T \mathbf{w})^k}{\sigma_d^{2k} k!} \hat{\mathbf{v}}(\mathbf{w}) = \exp\left(\frac{\mathbf{w}^T \mathbf{w}}{\sigma_d^2}\right) \hat{\mathbf{v}}(\mathbf{w}) = \hat{\mathbf{v}}_c(\mathbf{w}) \quad (8)$$

where the exponential appears from its Taylor series. Let $\sigma^2 = 2/\sigma_d^2$. The velocity \mathbf{v} is obtained by smoothing \mathbf{v}_c with the Gaussian kernel $G_\sigma = 1/\sqrt{2\pi\sigma^2}^d \exp(-\mathbf{x}^T \mathbf{x}/(2\sigma^2))$, d being the image dimension. We retrieve the demons regularisation. We verify that the higher σ_d^2 , the lower σ^2 and the less regularised the transformation: The width σ^2 of the Gaussian kernel corresponds to the strength of the regularisation σ_d^2 . It has to be noted that the derivation of (7) with respect to \mathbf{v} implies that all the spatial derivatives of \mathbf{v} vanish at the boundaries $\delta\Omega$ of Ω . Gaussian smoothing must be performed accordingly by extending the image periodically for instance or by ensuring that the moving structure stays far from the image boundaries.

Scale-space theory provides another interesting insight on the algorithm. As shown in (Nielsen et al, 1994), the Gaussian smoothing, which is now the exact minimiser of the regularisation energy $\mathcal{E}_{reg}(\mathbf{v})$, is also the solution of the Heat Equation. This further justifies why logDemons, and demons algorithms in general, are considered as diffusion registration methods (Pennec et al, 1999; Modersitzki, 2004; Cahill et al, 2009).

3.2 Elastic-Like LogDemons

The previous developments enable us to directly integrate elastic regularisation in logDemons framework. To preserve demons computational efficiency, we build a regulariser based on multi-order isotropic differential quadratic forms (IDQF)

whose minimiser is exactly computed using the separable elastic-like kernel filter proposed by (Cachier and Ayache, 2004). With the simplified Einstein convention, the k^{th} -order IDQF of a vector field \mathbf{v} is defined by:

$$Q_{el}^k(\mathbf{v}) = \alpha_k \partial_{i_1..i_k} \mathbf{v}_{i_{k+1}} \partial_{i_1..i_k} \mathbf{v}_{i_{k+1}} + \beta_k \partial_{i_1..i_k} \mathbf{v}_{i_{k+1}} \partial_{i_{k+1}..i_k} \mathbf{v}_{i_1} \quad (9)$$

α_k and β_k are scalar coefficients of \mathbb{R} , $\alpha_k \geq 0$ and $\beta_k \geq -\alpha_k$ to ensure the positiveness of Q_{el}^k . With $\alpha_k = 1/k!$ we recognise in the first term of Q_{el}^k the k^{th} term of the previous Tikhonov regulariser (5). Elasticity is thus obtained through the second term of Q_{el}^k . We define the elastic regularisation as:

$$\mathcal{E}_{reg}(\mathbf{v}) = \frac{1}{\sigma_x^2} \|\mathbf{v}_c - \mathbf{v}\|_{L_2}^2 + \int_{\Omega} \sum_{k=1}^{+\infty} \frac{Q_{el}^k(\mathbf{v})}{\sigma_d^{2k} \sigma_x^2} \quad (10)$$

From the functional derivatives:

$$\begin{aligned}\partial_{\mathbf{v}} (\partial_{i_1..i_k} \mathbf{v}_{i_{k+1}} \partial_{i_1..i_k} \mathbf{v}_{i_{k+1}}) &= (-1)^k \Delta^k \mathbf{v} \\ \partial_{\mathbf{v}} (\partial_{i_1..i_k} \mathbf{v}_{i_{k+1}} \partial_{i_{k+1}..i_k} \mathbf{v}_{i_1}) &= (-1)^k \Delta^{k-1} \nabla \nabla^T \mathbf{v}\end{aligned}$$

It follows the optimal condition:

$$\mathbf{v} + \sum_{k=1}^{\infty} \frac{(-1)^k}{\sigma_d^{2k}} \left[\alpha_k \Delta^k \mathbf{v} + \beta_k \Delta^{k-1} \nabla \nabla^T \mathbf{v} \right] = \mathbf{v}_c \quad (11)$$

which is solved in the Fourier domain. Note that when $k=1$, the energy becomes the first-order Lamé elastic equation. According to the identities

$$\begin{aligned}\mathfrak{F}(\Delta^k \mathbf{v}(\mathbf{x})) &= (-1)^k (\mathbf{w}^T \mathbf{w})^k \hat{\mathbf{v}}(\mathbf{w}) \\ \mathfrak{F}(\Delta^{k-1} \nabla \nabla^T \mathbf{v}(\mathbf{x})) &= (-1)^k (\mathbf{w}^T \mathbf{w})^{k-1} \mathbf{w} \mathbf{w}^T \hat{\mathbf{v}}(\mathbf{w})\end{aligned}$$

(11) is transformed as:

$$\left[\underbrace{\left(1 + \sum_{k=1}^{\infty} \frac{\alpha_k (\mathbf{w}^T \mathbf{w})^k}{\sigma_d^{2k}} \right)}_A \text{Id} + \underbrace{\left(\sum_{k=1}^{\infty} \frac{\beta_k (\mathbf{w}^T \mathbf{w})^{k-1}}{\sigma_d^{2k}} \right)}_B \mathbf{w} \mathbf{w}^T \right] \hat{\mathbf{v}}(\mathbf{w}) = \hat{\mathbf{v}}_c(\mathbf{w})$$

Since A and B are scalars, we can apply Sherman-Morrison inversion formula, which yields the closed form solution:

$$\hat{\mathbf{v}}(\mathbf{w}) = \underbrace{\left[\frac{1}{A} \text{Id} - \frac{1}{A} \left(\frac{B}{A + B \mathbf{w}^T \mathbf{w}} \right) \mathbf{w} \mathbf{w}^T \right]}_M \hat{\mathbf{v}}_c(\mathbf{w})$$

The optimal velocity field \mathbf{v} is therefore obtained by filtering in the Fourier domain the correspondence velocity \mathbf{v}_c with the filter M . Computational efficiency can be greatly improved by choosing the coefficients α_k and β_k such that M is separable. If $\alpha_k = 1/k!$, A is the Gaussian kernel found in the previous section. One can demonstrate (see Appendix B) that if β_k is defined by $\beta_0 = 0$, $\beta_k = \sum_{i=1}^k \gamma^i \sigma_d^{2i} / (k-i)!$ $\forall k \geq 1$

1 and $\gamma \in \mathbb{R}$, then the second term of the filter M is proportional to the Hessian of the Gaussian kernel $\exp(\mathbf{w}^T \mathbf{w} / \sigma_d^2)$. With $\sigma^2 = 2/\sigma_d^2$ and $\gamma = \sigma^2 \kappa / (\kappa + 1)$ we retrieve the elastic-like separable vector filter proposed by Cachier and Ayache (2004):

$$\mathbf{v} = \left(G_\sigma \text{Id} + \frac{\sigma^2 \kappa}{1 + \kappa} \mathcal{H} G_\sigma \right) \star \mathbf{v}_c = G_{\sigma, \kappa} \star \mathbf{v}_c \quad (12)$$

$\mathcal{H} G_\sigma(\mathbf{x})$ is the Hessian of the Gaussian kernel G_σ . When $\kappa = 0$, $G_{\sigma, \kappa=0}$ is the Gaussian filter and the elastic regularisation energy (10) is exactly the diffusion energy (7). It is therefore straightforward to switch regulariser.

As for diffusion regularisation, σ^2 controls the strength of the regularisation. The *elastic* parameter κ behaves like the Poisson ratio ν of the theory of elasticity by controlling the cross-effects of the smoothing between the vector components. Cachier and Ayache (2004) showed that the higher κ , the more incompressible the deformation. This property still holds here even though $G_{\sigma, \kappa}$ acts on velocities and not on deformations. Indeed, the stationary velocities \mathbf{v} are parameters of the deformations, their norm is directly related to the length of the deformations through $E(\phi) = (\int_0^1 \|\mathbf{v}(t)\|_V^2 dt)^{1/2} = \|\mathbf{v}(t=0)\|_V$, where V is the space of velocities. Smoothing $\mathbf{v}(t=0)$ thus amounts to smoothing ϕ . This is very different from fluid registration which regularises the infinitesimal increments i.e., the instant velocities $\mathbf{v}(t)$. However, elastic-like regularisation may not be sufficient to recover locally incompressible deformations. κ only controls incompressibility at a global scale as it is a global parameter. Furthermore, perfect incompressibility would be reached only when $\kappa \rightarrow \infty$. As a result, hard constraints must be used when strong incompressibility is required.

4 Incompressible LogDemons

A transformation ϕ is locally incompressible if its Jacobian determinant $|\nabla \phi|$ equals one. This non-linear constraint however is computationally demanding. For diffeomorphic transformations one can show that the condition on fluid motion holds: Integrating divergence-free velocities over time yields incompressible deformations (Evans, 1998). Making logDemons incompressible is thus achieved by constraining the velocity field \mathbf{v} to be divergence-free. This only alters the regularisation step as the optimisation stage optimises $\mathcal{E}(\mathbf{v}, \mathbf{v}_c)$ with respect to the correspondence velocity \mathbf{v}_c .

Helmholtz decomposition states that any velocity \mathbf{v} that vanishes at infinity can be uniquely decomposed in the sum of a divergence-free field and a curl-free field. Using variational calculus, Simard and Mailloux (1988) demonstrated that the Helmholtz decomposition projects \mathbf{v} onto the space of divergence-free vector field in the L_2 -norm sense. In this work, we employ a similar technique to integrate the divergence free constraint in the registration energy. Let p be a

scalar field of the Sobolev space $H^1(\Omega) = \{p \in L^2(\Omega) \mid \forall i \partial p / \partial x_i \in L^2(\Omega)\}$ that vanishes at infinity ($p \in H_0^1$). Minimisers of (10) (or (7) if $\kappa = 0$) under the divergence free constraint are optima of the Lagrange function:

$$\begin{aligned} \mathcal{P}_{\text{reg}}(\mathbf{v}, p) &= \frac{1}{\sigma_x^2} \|\mathbf{v}_c - \mathbf{v}\|_{L_2}^2 + \int_{\Omega} \sum_{k=1}^{+\infty} \frac{Q_{el}^k}{\sigma_x^2 \sigma_d^{2k}} \\ &\quad - \frac{2}{\sigma_x^2} \int_{\Omega} p \nabla \cdot \mathbf{v} \end{aligned} \quad (13)$$

Calculating the Gâteaux derivatives of (13) yields the two optimal conditions:

$$\nabla \cdot \mathbf{v} = 0 \quad (14)$$

$$\mathbf{v} + \sum_{k=1}^{\infty} \frac{(-1)^k}{\sigma_d^{2k}} (\alpha_k \Delta^k \mathbf{v} + \beta_k \Delta^{k-1} \nabla \nabla^T \mathbf{v}) = \mathbf{v}_c - \nabla p \quad (15)$$

with $p = 0$ at the boundaries $\delta\Omega$ of the image domain. The optimal velocity field \mathbf{v} is therefore computed by smoothing the right hand side of the previous equation, $\mathbf{g} = \mathbf{v}_c - \nabla p$, with the kernel $G_{\sigma, \kappa}$. To compute \mathbf{g} , we take the divergence of (15) under the optimal condition $\nabla \cdot \mathbf{v} = 0$. This yields the Poisson equation under 0-Dirichlet boundary conditions:

$$\Delta p = \nabla \cdot \mathbf{v}_c \in H^{-1}(\Omega) \quad (16)$$

where $H^{-1}(\Omega)$ is the dual of $H_0^1(\Omega)$ ¹. p can thus be computed independently of \mathbf{v} by solving (16). This is exactly the Helmholtz decomposition of \mathbf{v}_c . $\mathbf{g} = \mathbf{v}_c - \nabla p$ is the L_2 projection of \mathbf{v}_c to the space of divergence-free vector fields, as $\nabla \cdot \mathbf{g} = \nabla \cdot \mathbf{v}_c - \Delta p = 0$. ∇p is the orthogonal curl-free component. Ensuring divergence-free velocity fields thus consists in projecting the correspondence velocity onto the space of divergence-free vector fields and smoothing the result.

With this approach, the incompressibility constraint can be applied within a subdomain $\Gamma \subset \Omega$ only by defining $p \in H_0^1(\Gamma)$, $p = 0$ on Ω / Γ . This may be useful for tracking incompressible tissues localised in space, like the cardiac muscle. However, particular care must be taken at the domain boundaries $\delta\Gamma$. Although Gaussian smoothing theoretically preserves vector field divergence, in practice unconstrained velocities close to $\delta\Gamma$ may leak inside the incompressible domain due to the Gaussian convolution, ultimately resulting in volume drifts. Yet, Gaussian filter and vector derivatives commute for well-designed filters such as Deriche recursive filters (Deriche, 1993). We therefore replace the theoretical “project-and-smooth” strategy by a “smooth-and-project” approach that preserves the divergence close to $\delta\Gamma$. To further limit numerical instabilities, a smooth domain

¹ In the continuous domain, one would need p to be twice differentiable in order to compute the Laplacian. H_0^1 is sufficient in practice as (16) is solved on a discrete grid, the Laplacian being computed on discrete points which can be seen as delta Dirac. The Sobolev space of distributions $H^{-1}(\Omega)$ is thus sufficient to calculate Δp .

transition is implemented in a narrow band around Γ by diffusing the pressure field p using heat-transfer equation (Evans, 1998). The main steps of the proposed algorithm, henceforth termed *iLogDemons*, are summarised in (Algorithm 2). Note that incompressibility can be easily disabled by skipping the steps 6 and 7 of the algorithm.

Algorithm 2 iLogDemons: Incompressible Elastic LogDemons Registration

Require: Stationary velocity field \mathbf{v}^0 . {Usually $\mathbf{v}^0 = \mathbf{0}$ i.e. $\phi^0 = \text{Id}$ }.

- 1: **loop** {over n until convergence}
- 2: Compute the update velocity: $\delta\mathbf{v}^n$ given \mathbf{v}^{n-1} (3).
- 3: Fluid-like regularisation: $\delta\mathbf{v}^n \leftarrow G_{\sigma_f} * \delta\mathbf{v}^n$, G_{σ_f} is a Gaussian kernel.
- 4: Update the correspondence velocity: $\mathbf{v}^n \leftarrow Z(\mathbf{v}^{n-1}, \delta\mathbf{v}^n)$ (4).
- 5: Elastic-like regularisation: $\mathbf{v}^n \leftarrow G_{\sigma, \kappa} * \mathbf{v}^n$ (12)
- 6: Solve: $\Delta p = \nabla \cdot \mathbf{v}^n$ with 0-Dirichlet boundary conditions (18)
- 7: Project the velocity field: $\mathbf{v}^n \leftarrow \mathbf{v}^n - \nabla p$.
- 8: **end loop**
- 9: **return** \mathbf{v} , $\phi = \exp(\mathbf{v})$ and $\phi^{-1} = \exp(-\mathbf{v})$.

About Divergence-Free Update Velocity One could also constrain the correspondence field ϕ_c to be incompressible in order to find the optimal image matching that satisfies the constraint (see Appendix C). When the transformation ϕ is incompressible, it follows from the diffeomorphic update rule $\phi_c \leftarrow \phi \circ \exp(\delta\mathbf{v})$ that ϕ_c is incompressible if $\delta\mathbf{v}$ is divergence-free. Yet, from a theoretical perspective, adding such a constraint to the iLogDemons would have little effect on the result. In theory, constraining \mathbf{v} to be divergence-free amounts to projecting \mathbf{v}_c to the space of divergence-free vector fields. ϕ_c is therefore incompressible. Since the composition of two continuous incompressible fields is incompressible, $\exp(\delta\mathbf{v})$ is also incompressible and $\delta\mathbf{v}$ is divergence-free. When the zeroth order BCH approximation is used to compute \mathbf{v}_c , the linearity of the projector yields the same conclusion. The two approaches are hence equivalent. Yet, small differences may arise in practice due to the numerical approximations - scaling-and-squaring integration, numerical accuracy of the composition, etc. We will experimentally evaluate when it is necessary to add such a constraint.

Numerical Implementation The algorithm has been implemented using ITK and the open source implementation of the log-domain demons (Dru and Vercauteren, 2009). The Poisson equation (16) is discretised on the image grid using finite difference schemes (Simard and Mailloux, 1988) as the incompressible domain Γ may be of irregular shape. Its resolution is performed using PETSc library. Should incompressibility be ensured over the entire image domain Ω , more efficient Fourier techniques can be preferred (Hinkle et al, 2009).

5 Experiments and Results

Three experiments were performed to evaluate how much iLogDemons improves the recovery of incompressible deformations with respect to the original logDemons.

1. We first tested on synthetic datasets the ability of the elastic regularisation alone to estimate random incompressible deformations.
2. We then tested extensively the incompressibility constraint on large analytic incompressible transformations to quantify the improvements with respect to logDemons.
3. We finally applied the iLogDemons to estimate left ventricular myocardium motion from multi-slice short axis cine magnetic resonance images (cMRI). The results were compared with logDemons using tagged MRI (tMRI) measurements as reference.

In the following, *logDemons* refers to the unconstrained logDemons algorithm, either with diffusion or elastic-like regularisation (Algorithm 1). *iLogDemons* refers to the proposed incompressible logDemons algorithm, where the velocities \mathbf{v} are constrained to be divergence-free (Algorithm 2). We also evaluated the fully constrained iLog-Demons, where both the update velocities $\delta\mathbf{v}$ and the velocity \mathbf{v} are divergence-free. This algorithm is called *i²LogDemons*.

5.1 Global Incompressibility Recovery Using Elastic Regularisation

As we have seen, elastic regulariser theoretically provides more incompressible deformation fields, controlled by the global parameter κ . Here, we experimentally test how much this feature alone (no incompressibility constraint) can help in recovering random incompressible deformation fields.

5.1.1 Illustration on Translated Cubes

We first tested the elastic-like regularisation on a toy example to have an intuition of the results. Two translated black-and-white small cubes were co-registered using diffusion ($\sigma^2 = 1, \kappa = 0$) and elastic-like ($\sigma^2 = 1, \kappa = 0.5$) regularisation. As illustrated in Fig. 1, the elastic-like regularisation yielded deformations globally more incompressible as it distributed the smoothing across deformation components. The compressions around the cube were decreased, propagated over the image domain.

5.1.2 Quantitative Evaluation on Random Incompressible Deformations

How much the elastic-like regularisation can help in estimating incompressible deformations was quantified on synthetic data sets generated as follows. A 3D isotropic Steady-

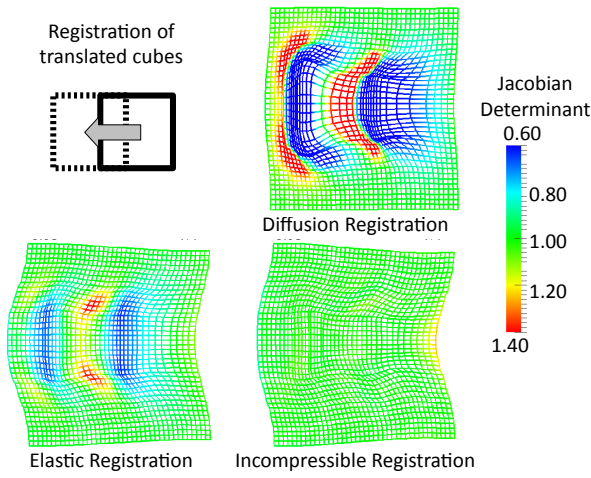


Fig. 1 Registration of two translated cubes using diffusion logDemons, elastic-like logDemons and iLogDemons. At similar grey level RMSE, elastic-like regularisation yielded stiffer deformations by distributing the compressions around the square over the image domain. iLogDemons yielded incompressible deformation closer to the true translation.

State Free Precession (SSFP) MR image of the heart, henceforth called test image, was warped by 50 random incompressible deformation fields. Warped and test images were then altered with slight Gaussian noise (SD= 3, range of grey level intensities: [0 : 198]) (Figure 2A-B).

The random deformation fields were generated by integrating divergence-free velocity fields. Each voxel was assigned a random velocity according to a Gaussian distribution with high standard deviation to get large displacements and large strains (SD= 5000mm/s). The resulting velocity field was smoothed with a Gaussian kernel (SD= 3mm) and its L_2 -norm was normalised to 2mm. We then made it divergence-free using Helmholtz decomposition and integrated the result with the “scaling-and-squaring” algorithm (Appendix A) to get the final incompressible deformation (Figure 2C). The average L_2 -norm of the deformation fields was $1.83 \pm 0.77\text{mm}$ (mean \pm standard deviation SD). Their Jacobian determinant was and 0.99 ± 0.03 , very close to the incompressibility condition $|\nabla\phi| = 1$ (Figure 2D). Besides, we verified with this procedure that “scaling-and-squaring” divergence-free velocity fields do yield near incompressible deformations. Indeed, directly integrating the original non divergence-free velocities yielded deformations with similar L_2 -norm ($1.91 \pm 0.99\text{mm}$) but that did not preserved volume ($|\nabla\phi| = 1 \pm 0.53$).

We registered the 50 warped images to the test image with and without elastic regularisation. The following registration parameters were used, $\sigma_f^2 = 1$, $\sigma^2 = 1$ and $\sigma_x = 1$, and no multi-resolution scheme was used as we aimed at comparing two methods rather than pure performances. The number of demons iterations was fixed to 50. Several elastic parameter values were tested $\kappa = \{0, 0.1, 0.5, 1, 2, 10, 100\}$.

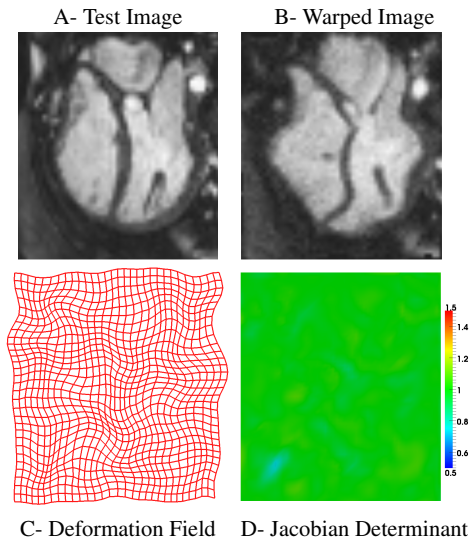


Fig. 2 Examples of synthetic 3D images and random incompressible deformation fields represented by a warped grid.

Registration accuracy was measured using the distance to the true deformation field (DTF) and the relative mean squared error of image intensities (RMSE) defined by:

$$\text{DTF}(\phi, \phi_{ref}) = \|\phi - \phi_{ref}\|_{L_2}$$

$$\text{RMSE}(T, R \circ \phi) = \|T - R \circ \phi\|^2 / \|T - R\|^2$$

For both indices, the lower the value, the better. Variations in registration performances were quantified using the coefficients of variation $v = \text{mean}/\text{sd}$ of RMSE, DTF and Jacobian determinant. Low v values mean little impact of the elastic regularisation on a particular metric.

The results showed that deformation field recovery and image matching accuracy did not change significantly by increasing κ ($v_{\text{DTF}} \approx 1.6\%$, $v_{\text{RMSE}} \approx 8.5\%$, Fig. 3). However, increasing κ largely reduced the standard deviation of the Jacobian determinant ($v_{\text{std(Jac.)}} \approx 36\%$) while its mean was close to one ($v_{\text{mean(Jac.)}} \approx 0.18\%$). The elastic regularisation thus improved global incompressibility of the deformation. However, it did not change the local accuracy of the registration. Strong constraints are needed to better recover locally incompressible deformations.

5.2 Local Incompressibility Recovery Using Volume-Preserving Constraint

In the previous experiment we have seen that elastic regularisation alone is not sufficient to accurately recover locally incompressible deformations. We now evaluate how much the incompressibility constraint, without elastic regularisation, can recover locally but strong volume-preserving deformation fields.

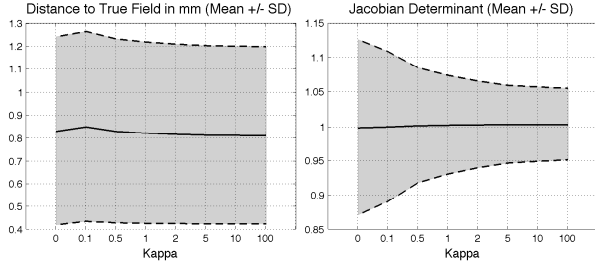


Fig. 3 Effect of elastic-like regularisation on registration performances. These curves show that elastic regularisation, controlled by the parameter κ , does not affect registration accuracy (low variation of distance to true field, left panel) while it significantly decreases Jacobian determinant standard deviation (right panel). The deformation is globally more incompressible.

5.2.1 Illustration on Translated Cubes

As for the elastic regularisation, we first tested the incompressibility constraint on the small cubes to get an intuition of the results. Elastic regularisation was disabled ($\sigma^2 = 1$, $\kappa = 0$) and the incompressibility constraint was turned on. As one can see in Fig. 1, the incompressibility constraint also prevented the compressions around the cubes as the elastic regulariser. Yet, the true global translation was qualitatively better recovered.

5.2.2 Quantitative Evaluation on Analytic Incompressible Whirls

We quantified the previous qualitative observation on synthetic data generated by warping the test image with analytic whirl transformations (Fig. 4). We decided not to use the previous synthetic dataset to avoid any bias as the deformations were generated using divergence free velocities, like the proposed constraint. Furthermore, analytic whirls enable working on much stronger but still volume-preserving deformations.

8 volume preserving whirl transformations were created as in (Saddi et al, 2007). The voxel O at the centre of the image domain was the centre of the whirl. All the voxels P that were outside the sphere of radius R and centred in O did not move. The voxels P inside the sphere were rotated with respect to O with an angle $\alpha(P) = \alpha_0(1 - \text{dist}(P, O)/R)^2$. The strength of the deformation was controlled by the whirl angle α_0 , spanning from 10° to 80° . Within the whirl domain, the L_2 -norm varied from 0.52 mm to 4.78 mm but the Jacobian determinant remained close to one (worst value: $|\phi_{\alpha_0=80^\circ}| = 1 \pm 0.04$).

The 8 images T warped using the whirl transformations ϕ_{α_0} were registered to the test image R using LogDemons and iLogDemons ($\sigma_x = 1$, $\sigma^2 = 1$, $\sigma_f^2 = 1$, $\kappa = 0$, number of iterations fixed to 150 to ensure convergence at any whirl angle). RMSE, Jacobian determinant and DTF are reported

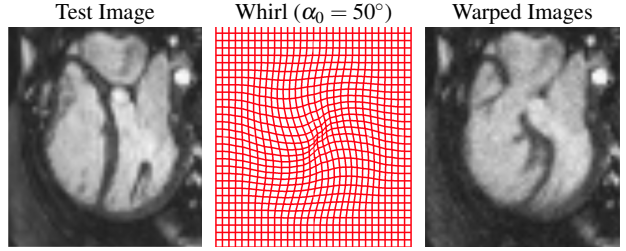


Fig. 4 Examples of synthetic 3D images and whirl deformations fields represented by a warped grid.

in Fig. 5. As expected, the deformation fields estimated with iLogDemons were almost incompressible. Jacobian determinants were always equal to 1 ± 0.02 independently of the strength of the whirl to recover. Image matching accuracy was not affected by the incompressibility constraint, showing only 0.6% decrease. Most importantly, iLogDemons significantly improved the accuracy of the recovered deformation fields. Means and standard deviations of DTF were systematically lower (average improvements of 29% and 36% respectively). The larger the deformation, the more significant the improvement while RMSE stayed comparable. This experiment demonstrated the importance of the transformation model. As illustrated in Fig. 6, regions with homogeneous grey levels provided few information to accurately estimate the whirl. With the iLogDemons, the incompressibility constraint helped the algorithm by ensuring that the estimated deformation is of the same type as the true field. This feature is particularly interesting for clinical applications, where deformations must be reliably estimated from ill-textured images. In particular, we observed that iLogDemons provided significantly more accurate results than the original algorithm in images with very large slice thicknesses (see Appendix D for results on synthetic data).

We also investigated if the performances were improved using $i^2\text{LogDemons}$, which also enforces the update velocity field to be divergence-free (Appendix C). Results, reported in Fig. 5, were in agreement with the theoretical considerations (Sec. 4). Relevant differences only appeared at large deformations ($\alpha_0 \geq 70^\circ$). Finally, it should be noted that all these observations continue to hold with $\sigma_x = 2, 4$ and on random incompressible fields (experiments non reported here), supporting robustness to parameters.

To conclude, the experiments on synthetic data showed that 1) elastic regularisation does provide globally more incompressible deformation fields but does not significantly improve the local accuracy of the registration; 2) the proposed strong incompressibility constraint provides almost incompressible deformations and do improve the recovery of volume preserving deformations. Both contributions are therefore complementary and can be used jointly to obtain smooth, globally and locally incompressible deformation fields.

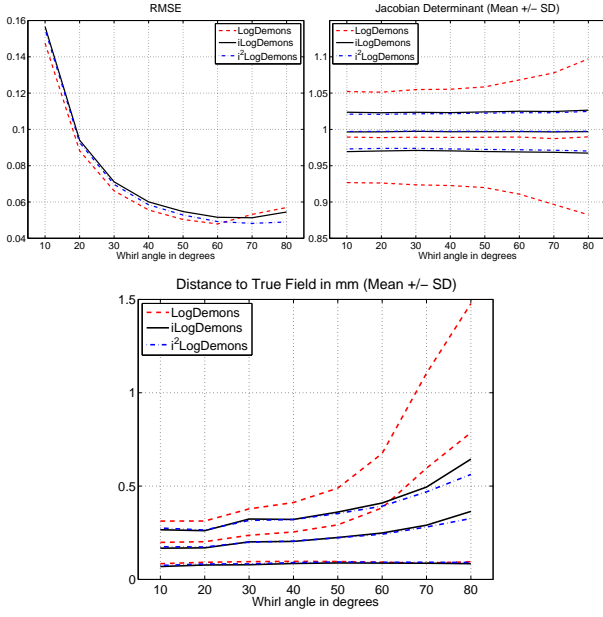


Fig. 5 Results of the registration of whirl datasets. With similar image matching performances (similar RMSE of image intensities, *top-left panel*), iLogDemons provided more incompressible deformations (Jacobian determinant closer to one, *top-right panel*) and outperformed LogDemons in terms of deformation field accuracy (lower DTF, *bottom panel*). Constraining the update velocity to be divergence-free (i^2 LogDemons) did not improve the results significantly.

In the next section we evaluate the proposed algorithm in a concrete clinical situation.

5.3 Application to Cardiac Deformation Recovery

As a feasibility study, we applied iLogDemons to estimate the 3D strain of the left-ventricular cardiac muscle, the myocardium, from standard anatomical cine MR image (cMRI) of the heart (Fig. 7). Widely available in clinical routine, these images have good in-plane and temporal resolutions. However, they only show the apparent motion of the heart as no texture is present within the myocardium. Combined with their large slice thickness, accurate estimation of cardiac motion from cMRI is a challenging task. During the cardiac cycle, it has been reported that the volume of the heart muscle does not vary significantly ($\approx 5\%$ of volume variation (Glass et al, 1991)). It is therefore reasonable to use incompressibility constraints to estimate cardiac motion (Bistoquet et al, 2008). We thus applied iLogDemons to estimate 3D myocardium strain on cMRI of two adult patients with heart failure. Results were compared with those obtained using logDemons and the ground truth provided by tagged MRI.

Image Acquisition and Preparation Anatomical cMRI were acquired in the short axis view with multiple breath-holds

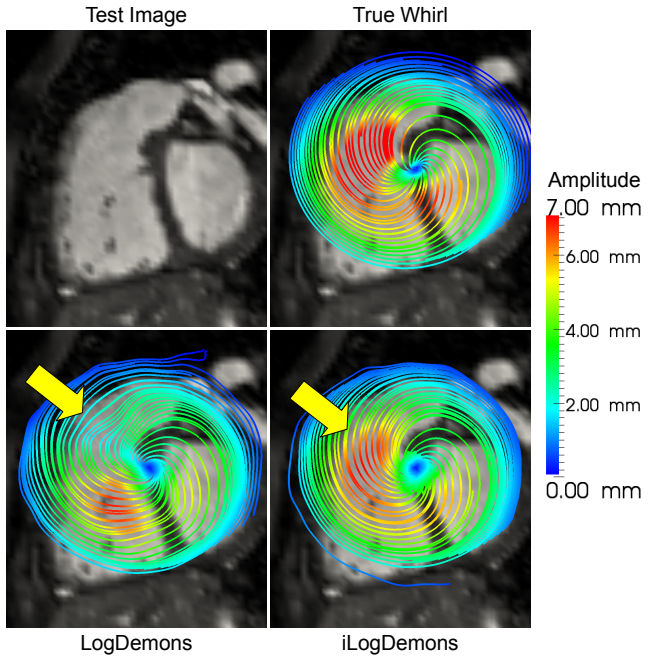


Fig. 6 Streamlines of true and estimated whirl deformations ($\text{whirl angle } \alpha_0 = 60^\circ$). Colours encode deformation amplitude in mm. iLogDemons better estimate the whirl transformation in regions with poor texture (yellow arrow), providing more accurate motion and deformation amplitude.

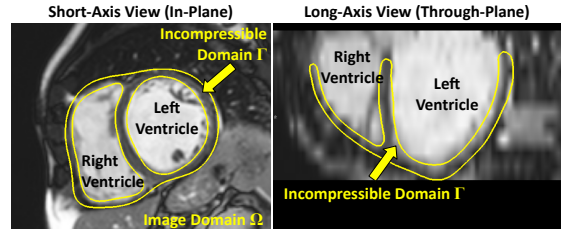


Fig. 7 Short-axis cine-MRI of patient 1. Incompressibility is ensured only within the myocardium (outlined in yellow). Note the lack of consistent texture within the myocardium even in the in-plane image (*left panel*) and the coarse through plane resolution (*right panel*).

(Achieva, Philips Medical System, 30 time frames, 1.4mm^2 isotropic in-plane resolution, 10mm slice thickness). For the first patient, 3D tagged MR images (tMRI) were acquired during the same exam (CSPAMM encoding, 23 time frames, 1.0mm^3 isotropic resolution, tag size $\approx 7\text{mm}$, Fig. 9 left panel). No manual tracking of the tag grids was available since this task is extremely difficult due to the 3D nature of the motion. For the second patient, 2D tMRI were acquired in the short axis view (23 time frames, 1.1mm^2 in-plane resolution, 18mm slice thickness, tag size $\approx 6\text{mm}$). For this case, manual tracking of the tag grids was performed by an expert in the short axis view. All images fully covered both ventricles. The two cMRI and the 3D tMRI presented no slice misalignments. The tMRI were spatially and temporally aligned to the cMRI using DICOM information. Fi-

nally, the dense transformations were defined on an isotropic sampling grid adjusted to the image dimensions to cope with the large slice thickness that can introduce high frequencies in the transformations, resulting in numerical instabilities and lower registration accuracy. In practice, this amounts to linearly resampling the cMRI to get isotropic voxels.

Tracking Protocol Because the transformations provided by demons algorithm are resampling fields, myocardium motion was estimated by recursively registering all the frames of the cardiac sequence to the end-diastole (ED) time frame as in (Mansi et al, 2009) (Fig. 8), when the heart is at rest position. Registration parameters were fixed: $\sigma_x = 1$, $\sigma^2 = 2$, $\sigma_f^2 = 0.5$. A 2-level multi-resolution scheme was used and registration was stopped as soon as RMSE stopped decreasing. For iLogDemons, elastic regularisation ($\kappa = 1$) was applied everywhere in the images whereas the incompressibility constraint was applied only within the myocardium as the volume of surrounding structures like blood pools vary (Fig. 7). Thanks to the backward strategy, myocardium region had to be defined only at the ED time frame. Finally, the 3D displacements and strains were projected onto the radial, circumferential and longitudinal directions as defined in (Moore et al, 2000) (Fig. 9, right panel). Strains were computed using the 3D Lagrangian finite strain tensor $E(\mathbf{x}) = \frac{1}{2} [\nabla \mathbf{u}(\mathbf{x}) + \nabla \mathbf{u}^T(\mathbf{x}) + \nabla \mathbf{u}^T(\mathbf{x}) \nabla \mathbf{u}(\mathbf{x})]$, where $\mathbf{u}(\mathbf{x})$ is the displacement at \mathbf{x} .

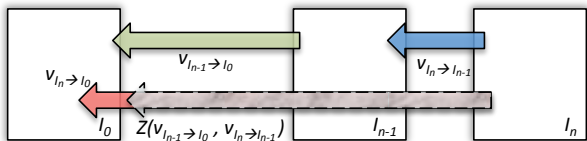


Fig. 8 Recursive tracking algorithm. Knowing the velocity $v_{I_{n-1} \rightarrow I_0}$ (green): 1) Estimate $v_{I_n \rightarrow I_{n-1}}$ (blue). 2) Concatenate $v_{I_n \rightarrow I_{n-1}}$ and $v_{I_{n-1} \rightarrow I_0}$ (grey) using BCH formula (4). 3) Estimate $v_{I_n \rightarrow I_0}$ using 2 as initialisation (red).

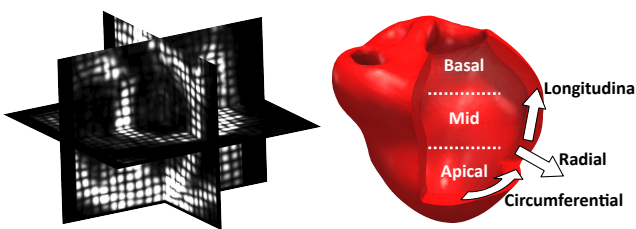


Fig. 9 Left panel: 3D tMRI of patient 1. Right panel: Definition of cardiac motion directions and heart regions.

Comparison with 3D tMRI In a first stage, we estimated the cardiac motion of patient 1 by tracking the heart in the 3D

tMRI using both iLogDemons and logDemons. We verified that iLogDemons preserved the volume of the myocardium below the values reported in the literature during the entire cardiac cycle (average volume variation: 2%, max.: 6%) contrary to logDemons (average volume variation: 26%, max.: 32%) (Fig. 10, top-left panel). We also observed that the incompressibility constraint reduced the deviations of the estimated motions along the cardiac cycle despite the simple tracking procedure.

For visual assessment, we applied the estimated deformations to virtual planes manually positioned at ED (Fig. 11). Realistic deformations consistent with the tag grids were obtained with both algorithms. The similar performances between logDemons and iLogDemons, quantified by the low L_2 -distance between recovered deformation fields (Table 1), is justified by the fact that the tag grids provided enough texture information within the myocardium to guide the registration. As no ground truth was available, we considered the motion estimated on the 3D tMRI using iLogDemons as reference.

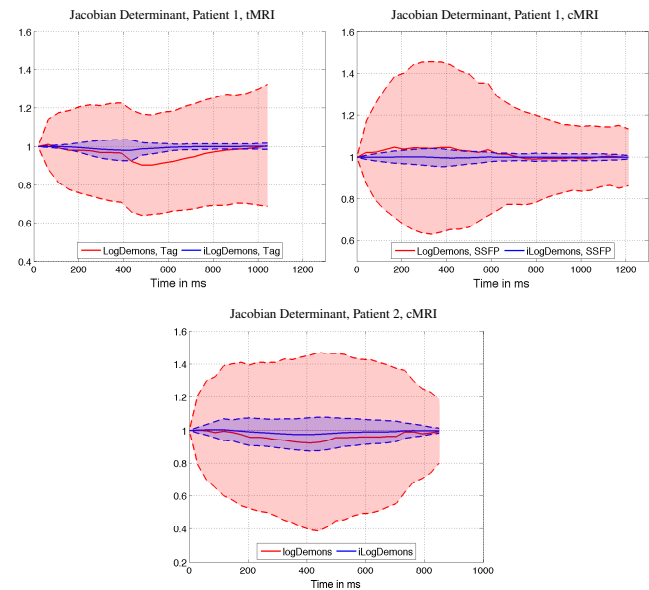


Fig. 10 Jacobian Determinant of Myocardium Motion Incompressibility constraint significantly decreased volume variations during the cardiac cycle. One can observe that the constraint also controlled the volume deviation at the end of the cycle (see the 3D tMRI).

We then estimated the 3D motion of the heart from the cMRI and compared the results with the reference tMRI deformation. Visual assessment of the warped virtual planes showed that the incompressibility constraint did help in recovering longitudinal and circumferential motion despite the large slice thickness and the lack of texture hints within the myocardium (Fig. 11, blue and red curves, Table 1). Estimated longitudinal and circumferential strains confirmed

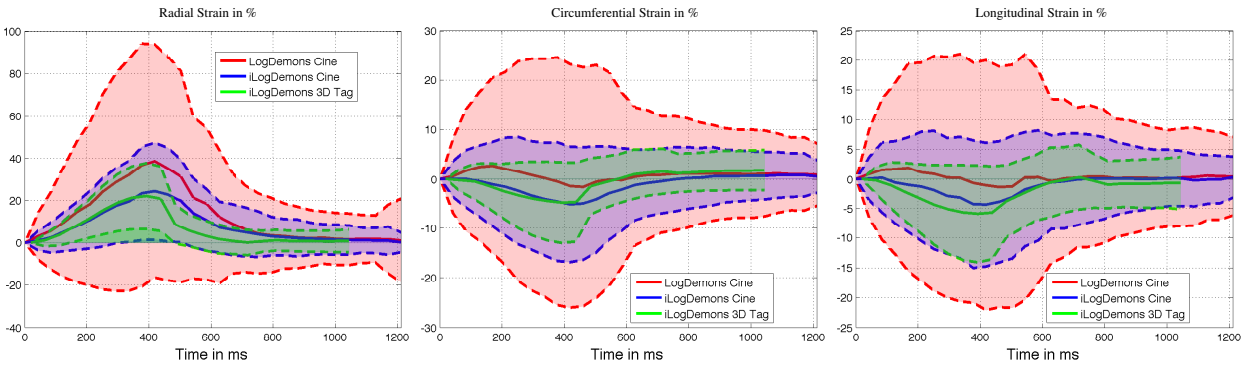


Fig. 12 Myocardium strains computed from cMRI and 3D tMRI of patient 1. Mean and standard deviation computed over the entire left ventricle. iLogDemons better estimated circumferential and longitudinal strains despite the lack of image information and the large slice thickness.

this finding (Fig. 12). Values obtained using iLogDemons were much closer to the reference ($\approx 90\%$ of improvement for radial and circumferential strain respectively, 64% for longitudinal strain). The amplitude of the radial strain was more plausible and the temporal variation patterns of the circumferential and longitudinal strains were consistent with the clinical literature (Moore et al, 2000). Note that logDemons exhibited a wrong lengthening in both longitudinal and circumferential directions at the beginning of the cardiac contraction. Furthermore, the variability in strain measurements is significantly reduced using iLogDemons, which suggests that the estimated motion is globally more consistent.

Table 1 L_2 -distances averaged over the cardiac cycle between estimated displacements. Values to be compared with the tag size: 6mm. Tracking cardiac motion on tMRI with logDemons and iLogDemons yielded globally little differences. When tracking the heart on cMRI, iLogDemons improved the results thanks to the incompressibility constraint that accommodate the lack of myocardial texture and the large slice thickness.

Method	L_2 -distance (mean \pm sd, max)
iLogDemons (tMRI)	reference
logDemons (tMRI)	$1.7 \pm 0.71\text{mm}, 3.2\text{mm}$
logDemons (cMRI)	$3.2 \pm 0.92\text{mm}, 4.6\text{mm}$
ilogDemons (cMRI)	$2.8 \pm 0.72\text{mm}, 4.0\text{mm}$

Comparison with Manual Tracking We then estimated the cardiac motion of the second patient using logDemons and iLogDemons on cMRI and compared the results with manual tracking of 2D tag grids. As with the previous patient, iLogDemons controlled myocardium volume variations all along the cardiac cycle compared to logDemons (average volume variation: 7%, max.: 10%, and 42%, max.: 54% respectively, Fig. 10). Point-wise motion comparison between cMRI and manual tracking was not possible due to a non-perfect tMRI-to-cMRI alignment because of tMRI slice misalignment and patient motion between scans. We thus com-

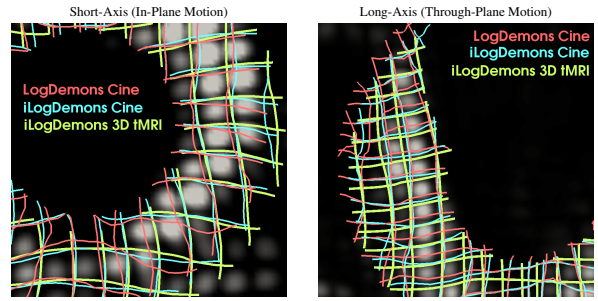


Fig. 11 Close-up of the tMRI of patient 1 at end-systole. The virtual tag planes were warped with the deformation estimated on the tMRI using iLogDemons (green) and with those estimated on the cMRI using logDemons (red) and iLogDemons (blue). The green planes show that the motion estimated on tMRI using iLogDemons was very similar to the MRI tags. From the blue and red planes one can see that iLogDemons better estimated myocardium motion even in cMRI.

pared the regional displacements averaged over 12 heart zones (6 basal and 6 mid-ventricular regions). Note that the slice misalignments of the tMRI did not affect the evaluation as the measurements were exclusively 2D. For fair comparison, we transformed the 3D displacements estimated from the cMRI to apparent 2D motions by warping the short-axis displacement (XY-plane) along the through plane motion (Z-direction). The results showed that iLogDemons, in this patient, improved the accuracy of the recovered motions. The amplitude of the radial motion was closer to the ground truth (global error with respect to tag displacements from $2.4 \pm 2.4\text{mm}$ to $1.2 \pm 1.6\text{mm}$, about the voxel size, Fig. 13). Note that logDemons already estimated realistic radial motion patterns, yet over-estimated, as the apparent cardiac displacements in cMRI are radial to the LV boundaries. The circumferential motion provided by iLogDemons was more realistic than the one estimated using logDemons, yet still under-estimated (global error from $2.3 \pm 1.7\text{mm}$ to $3.5 \pm 2.0\text{mm}$, Fig. 14). The sign and dynamics of the average circumferential displacement were correctly recovered for every region except for regions 8 and 12, whereas logDemons

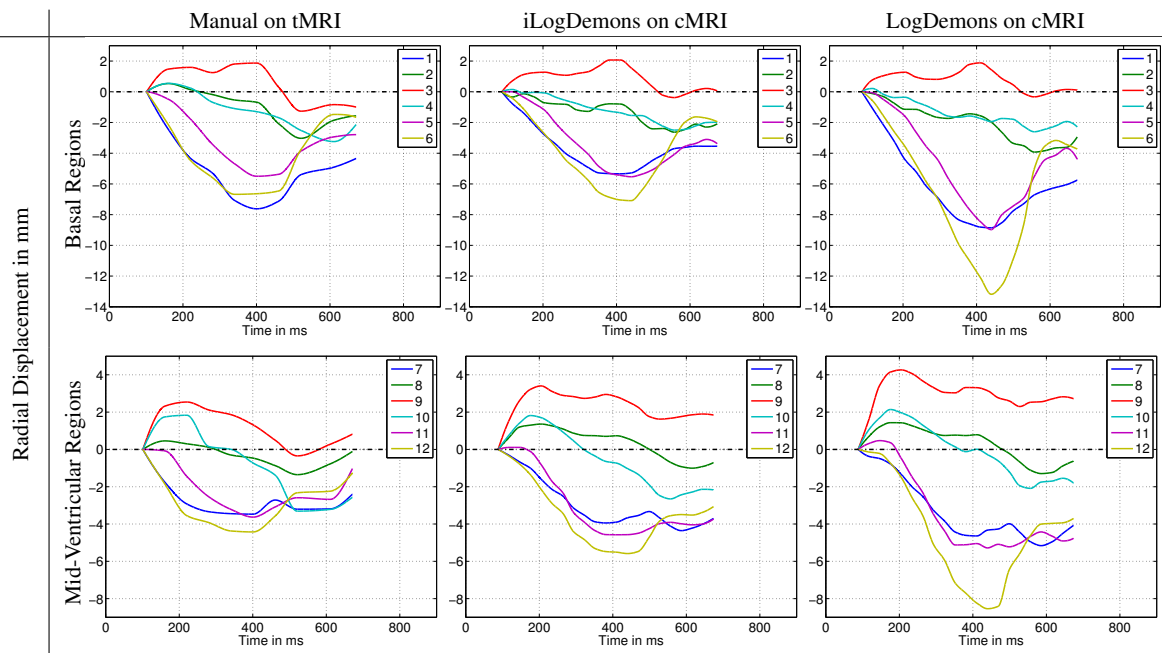


Fig. 13 Basal and mid-ventricular radial displacements of patient 2 (in mm, averaged per LV zone). Compared with the radial displacements measured by an expert on tMRI (left panels), the displacements estimated on cMRI using iLogDemons (mid panel) had more realistic amplitudes compared with those estimated with logDemons (right panels). Note that both algorithms recovered realistic radial motion patterns over the cardiac cycle as the image gradients of the cMRI are sufficient to estimate the thickening of the heart.

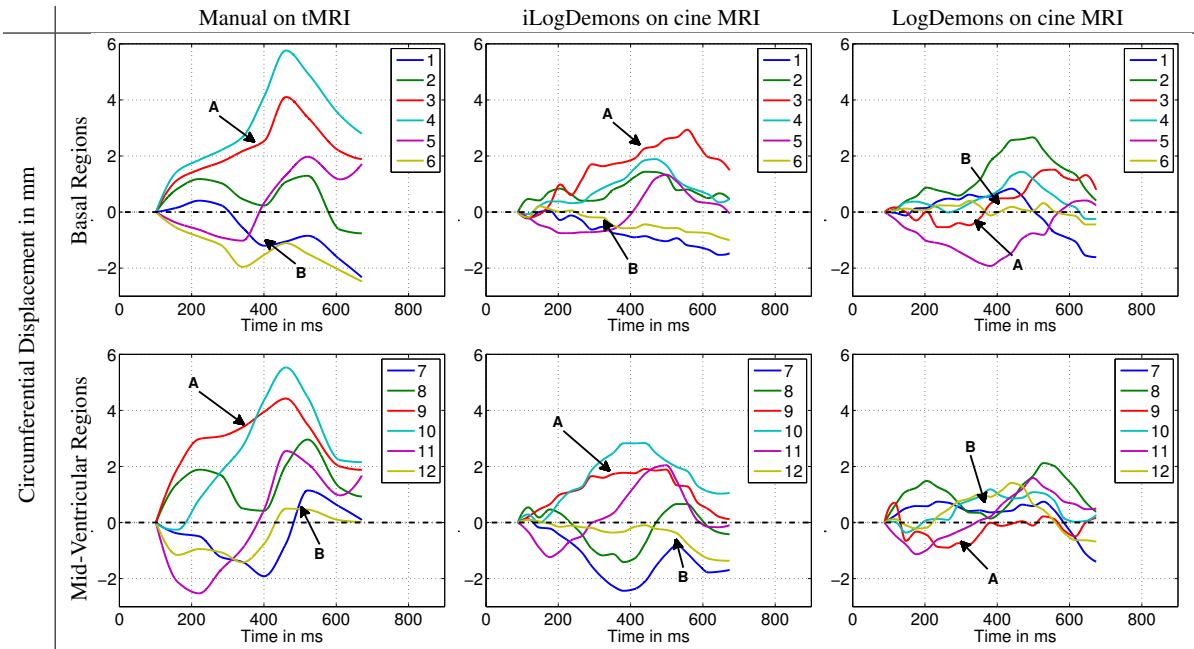


Fig. 14 Basal and mid-ventricular circumferential displacements of patient 2 (in mm, averaged per LV zone). Limited by the lack of consistent texture information, the circumferential displacements of the heart estimated on cMRI using both logDemons (right panel) and iLogDemons (mid panel) were globally under-estimated when compared to manual tracking on tMRI (left panel). Yet, iLogDemons motions presented more realistic patterns, as highlighted by the directions of the displacements of zones 9-10 (A) and zones 7-12 (B) for instance.

failed to estimate the circumferential motion of most of the regions (arrows A and B in Fig. 14). The incompressibility constraint assisted the registration algorithm by redistribut-

ing the apparent radial displacement across the other direction to preserve myocardium volume.

6 Discussion and Conclusion

In this article, we presented a method for elastic incompressible diffeomorphic registration based on the logDemons algorithm proposed by Vercauteren et al (2008). We first established that logDemons Gaussian regularisation minimises an infinite order Tikhonov regulariser. Our formulation constitutes a first well-posed formulation of demons algorithm with controlled parameters. An important theoretical condition on the coupling term $\|\log(\phi^{-1} \circ \phi_c)\|^2$ appeared. One must be able to linearise this term such that the regularisation energy is written as a least-square problem to justify the Gaussian regularisation. Equipped with a closed form expression of demons regularisation, we adapted it to elastic registration by replacing the Tikhonov regulariser with the infinite sum of isotropic differential quadratic forms whose minimiser is exactly computed through convolution with the separable elastic-like vector filter proposed by Cachier and Ayache (2004). We then enforced the algorithm to provide incompressible deformations by constraining the search space of stationary velocities to the space of divergence-free vector fields. In practice, this is achieved by adding a new term to the deformation field estimated by the logDemons. The constraint can therefore be enabled/disabled at user will, no ad-hoc minimisation schemes are required. Compared with traditional methods, our approach is well posed, it provides diffeomorphic transformations, it introduces only one extra parameter related to the elasticity of the transformation and the incompressibility constraint requires no parameter and can be applied within a localised area of the image only.

The synthetic experiments demonstrated that the proposed elastic-like regulariser provides realistic elastic deformations with infinite order of smoothness. Contrary to more traditional approaches based on the linear Lamé equation (Modersitzki, 2004), our method relies on separable vector filters that can be implemented using efficient Gaussian filters (Deriche, 1993). As it relies on a kernel, our technique may recall spline-based elastic registration algorithms (Sorzano et al, 2005). However, the transformation provided by the iLogDemons are diffeomorphic and computed everywhere in the image.

In this paper, we used isotropic elastic regularisation to estimate myocardium deformation. Because the cardiac muscle is anisotropic, that transformation model may not be perfectly adapted. Yet, designing efficient anisotropic smoothing is not straightforward and, in that case, it is even more challenged by the spatial variation of the cardiac anisotropy. We thus decided to use isotropic filters for the sake of efficiency but thanks to the proposed regularisation framework, more advanced anisotropic regularisation could be investigated in the future.

The synthetic experiments also supported the proposed incompressibility constraint. We showed that deformations

parameterised by stationary divergence-free velocities are very close to incompressibility despite the approximations and the numerical precision. The linearity of the divergence allows efficient implementation of the constraint, in contrast to previous approaches based on the non-linear determinant constraint that was quite time consuming (Rohlfing et al, 2003; Haber and Modersitzki, 2004). In all our experiments, the Jacobian determinant of the estimated deformations remained close to one independently of the strength of the deformations. We also showed that constraining the update velocities to be divergence-free at each iterations does not significantly improve the recovery of incompressible deformations.

Elastic incompressible registration has numerous clinical applications, from the registration of breast images (Rohlfing et al, 2003) to the tracking of the heart (Bistoquet et al, 2008). In this article, we presented how our approach could be used to estimate 3D myocardium strain from 3D tMRI and standard cMRI of the heart. We observed that enforcing incompressible elasticity significantly increased the realism and the accuracy of the estimated motions and strains. Recovered deformation fields were closer to the motions computed automatically or manually from tMRI. The possibility to apply the incompressibility constraint in a limited domain of the image has been crucial for this experiment, as only the myocardium is incompressible. Blood pool volume must vary to ensure correct registration. Moreover, as myocardium region is relatively small, little computational overhead is added to the logDemons algorithm.

However, some theoretical aspects still need to be consolidated. When the incompressibility constraint is applied within a limited subdomain of the image, smooth transitions are ensured by artificially diffusing the Lagrangian pressure field p . Intuitively, this technique would be equivalent to using a mask of the incompressible domain with smooth transitions. Experiments supported this approach as no numerical instabilities appeared. However, a rigorous formulation that explicitly integrates the mask into the registration energy functional would enable more efficient numerical schemes.

A second theoretical challenge to investigate is the viscous Gaussian regularisation of the update velocities $\delta\mathbf{v}$. Intuitively, this intermediate regularisation controls the regularity of the log-domain, which must be smooth enough to ensure that the integrated transformations are diffeomorphisms (Do Carmo and Flaherty, 1992). Although this step is optional, its use greatly contributes to the stability of the algorithm: A slight smoothing of the update velocities is recommended. It would be interesting however to develop a theoretical proof of this intuition to implement more sophisticated regularisation schemes, by endowing the space of velocity fields with a kernel norm for instance (Hernandez et al, 2009).

Numerically, our approach is relatively simple to implement as it is based on Gaussian filters and it requires solving a linear system with constant stiffness matrix. In this work the Poisson equation was solved in the space domain to be able to constrain incompressibility in regions of arbitrary shapes, which would have been difficult to achieve with Fourier techniques. Nevertheless, elastic-like divergence-free filters implemented in the Fourier domain could be more efficient for whole-domain incompressibility constraint, as in (Hinkle et al, 2009).

As additional future directions, it would be interesting to integrate our approach into registration methods based on time-varying velocity fields (Beg et al, 2005; Hinkle et al, 2009). From a clinical point of view, more sophisticated tracking strategies can be investigated to make the estimation of the myocardium motion more robust (Bistoquet et al, 2008; Sundar et al, 2009b). Current work aims at quantitatively validating the algorithm on MRI, 3D US and CT images of healthy subjects and patients suffering from severe congenital heart diseases and heart failure.

Acknowledgements The work has been partly funded by the European Commission through the IST-2004-027749 Health-e-Child Integrated Project (<http://www.health-e-child.org>). The authors would like to thank the King's College London, Division of Imaging Sciences, for the cine and tagged MR images, Aurélie Canale for manual tracking of tMRI and Dr. Jean-Marc Peyrat for fruitful discussions.

A Time-Integration of Stationary Velocity Fields

Arsigny et al (2006a) devised an efficient way to compute the exponential map of a stationary velocity field $\phi = \exp(\mathbf{v})$ by observing that, in virtue of the properties of one-parameter subgroups ($t \mapsto \exp(t\mathbf{v})$), we have $\forall n \in \mathbb{N}, \exp(\mathbf{v}) = \exp(\mathbf{v}/n)^n$. If n is large enough, $\exp(\mathbf{v}/n)$ can be approximated by \mathbf{v}/n (*scaling*), which is then composed $\log_2(n)$ times to get the exponential (*squaring*). The pseudo-code of the algorithm is:

Algorithm 3 Scaling-and-Squaring Algorithm

Require: Velocity field \mathbf{v}

- 1: Choose n such that $\|\mathbf{v}/2^n\| \leq 0.5$
- 2: Explicit first-order integration: $\mathbf{u} \leftarrow \mathbf{v}/2^n$
- 3: **loop** { n times}
- 4: $\mathbf{u} \leftarrow \mathbf{u} \circ \mathbf{u}$
- 5: **end loop**
- 6: **return** Displacement field \mathbf{u}

B IDQF Parameters for Separable Vector Filters

As described in Sec. 3.2, logDemons elastic-like regularisation is obtained by solving in the Fourier domain the optimal condition:

$$\left[\underbrace{\left(1 + \sum_{k=1}^{\infty} \frac{\alpha_k(\mathbf{w}^T \mathbf{w})^k}{\sigma_d^{2k}} \right)}_{A} \text{Id} + \underbrace{\left(\sum_{k=1}^{\infty} \frac{\beta_k(\mathbf{w}^T \mathbf{w})^{k-1}}{\sigma_d^{2k}} \right)}_{B} \mathbf{w} \mathbf{w}^T \right] \hat{\mathbf{v}}(\mathbf{w}) = \hat{\mathbf{v}}_c(\mathbf{w})$$

Sherman-Morrison inversion Lemma gives:

$$\hat{\mathbf{v}}(\mathbf{w}) = \underbrace{\left[\frac{1}{A} \text{Id} - \frac{1}{A} \left(\frac{B}{A + B \mathbf{w}^T \mathbf{w}} \right) \mathbf{w} \mathbf{w}^T \right]}_{M} \hat{\mathbf{v}}_c(\mathbf{w})$$

We seek α_k and β_k such that the filter M is separable to preserve demons computational efficiency. $\alpha_k = 1/k!$ yields $A = \exp(\mathbf{w}^T \mathbf{w} / \sigma_d^2)$. As a result, if $B/(A + B \mathbf{w}^T \mathbf{w})$ is a scalar $\gamma \in \mathbb{R}$, the inverse Fourier transform of the second term of M is the Hessian of $\mathfrak{F}^{-1}(\gamma \exp(-\mathbf{w}^T \mathbf{w} / \sigma_d^2))$. The idea thus consists in finding the coefficients β_k such that $B/(A + B \mathbf{w}^T \mathbf{w}) = \gamma$. With $\beta_0 = 0$, this writes:

$$\sum_{k=0}^{\infty} \frac{\beta_{k+1}}{\sigma_d^{2(k+1)}} (\mathbf{w}^T \mathbf{w})^k = \sum_{k=0}^{\infty} \gamma \left(\frac{1}{\sigma_d^{2k} k!} + \frac{\beta_k}{\sigma_d^{2k}} \right) (\mathbf{w}^T \mathbf{w})^k$$

This equation defines a recursive relationship between the β_k 's:

$$\begin{cases} \beta_0 = 0 \\ \beta_{k+1} = \gamma \left(\frac{\sigma_d^2}{k!} + \beta_k \right) \quad \forall k \geq 1 \end{cases}$$

from which we deduce the closed form:

$$\beta_k = \sum_{i=1}^k \frac{\gamma^i \sigma_d^{2i}}{(k-i)!}$$

The proof of this relationship is achieved by recurrence. The previous formula is verified for $k=1$. We assume it to be true for k and we verify it still holds for $k+1$. To this end, we replace β_k by the conjectured formula in the recursive expression of β_{k+1} :

$$\begin{aligned} \beta_{k+1} &= \sigma_d^2 \gamma \left(\frac{1}{k!} + \sum_{i=1}^k \frac{\gamma^i \sigma_d^{2i}}{(k-i)!} \right) = \frac{\gamma \sigma_d^2}{k!} + \sum_{i=1}^k \frac{\gamma^{i+1} \sigma_d^{2(i+1)}}{(k-i)!} \\ &= \frac{\gamma \sigma_d^2}{k!} + \sum_{i=2}^{k+1} \frac{\gamma^i \sigma_d^{2i}}{(k-(i-1))!} = \sum_{i=1}^{k+1} \frac{\gamma^i \sigma_d^{2i}}{(k+1-i)!} \end{aligned}$$

which proves the result. With these coefficients, the filter M writes:

$$\hat{\mathbf{v}}(\mathbf{w}) = (\exp(-\mathbf{w}^T \mathbf{w} / \sigma_d^2) \text{Id} - \gamma \mathbf{w} \mathbf{w}^T \exp(-\mathbf{w}^T \mathbf{w} / \sigma_d^2)) * \hat{\mathbf{v}}_c(\mathbf{w})$$

which becomes in the space domain (Δ is the Hessian operator and d is the dimension of the image domain Ω)

$$\begin{aligned} \mathbf{v}(\mathbf{x}) &= \sqrt{\sigma_d^2 / (4\pi)}^d \exp(-4\sigma_d^2 \mathbf{x}^T \mathbf{x}) * \mathbf{v}_c(\mathbf{x}) \\ &\quad + \gamma \Delta \left(\sqrt{\sigma_d^2 / (4\pi)}^d \exp(-4\sigma_d^2 \mathbf{x}^T \mathbf{x}) \right) * \mathbf{v}_c(\mathbf{x}) \end{aligned}$$

Defining $\sigma^2 = 2/\sigma_d^2$ and $\gamma = \sigma^2 \kappa / (1 + \kappa)$ yields (12).

C Demons Update Velocity under the Divergence-Free Constraint

Divergence-free update velocities are computed by minimising the constrained optimisation energy:

$$\begin{cases} \mathcal{E}_{cor}(\delta \mathbf{v}) = \frac{1}{\sigma_t^2} \|R - T \circ \phi \circ \exp(\delta \mathbf{v})\|_{L_2}^2 + \frac{1}{\sigma_x^2} \|\log(\phi^{-1} \circ \phi \circ \exp(\delta \mathbf{v}))\|_{L_2}^2 \\ \nabla \cdot \delta \mathbf{v} = 0 \end{cases}$$

Let $p(\mathbf{x})$ be a scalar field belonging to the Sobolev space $H_0^1(\Omega)$ that vanishes at infinity. The Lagrangian function $\mathcal{P}_{corr}(\delta\mathbf{v}, p)$ related to the constrained correspondence energy $\mathcal{E}_{corr}(\delta\mathbf{v})$ writes (the Lagrangian multiplier $p(\mathbf{x})$ has been multiplied by 2 to simplify calculations):

$$\begin{aligned}\mathcal{P}_{corr}(\delta\mathbf{v}, p) &= \frac{1}{\sigma_i^2} \int_{\Omega} \|R(\mathbf{x}) - T \circ \phi \circ \exp \delta\mathbf{v}(\mathbf{x})\|^2 d\mathbf{x} \\ &\quad + \frac{1}{\sigma_x^2} \int_{\Omega} \|\delta\mathbf{v}(\mathbf{x})\|^2 d\mathbf{x} - 2 \int_{\Omega} p(\mathbf{x}) \nabla \cdot \delta\mathbf{v}(\mathbf{x}) d\mathbf{x}\end{aligned}$$

Differentiating $\mathcal{P}_{corr}(\delta\mathbf{v}, p)$ with respect to p yields the constraint $\nabla \cdot \delta\mathbf{v} = 0$. To differentiate $\mathcal{P}_{corr}(\delta\mathbf{v}, p)$ with respect to $\delta\mathbf{v}$, we linearise the similarity criterion as in (Vercauteren et al, 2009):

$$\|R(\mathbf{x}) - T \circ \phi \circ \exp \delta\mathbf{v}(\mathbf{x})\|^2 \approx \|R(\mathbf{x}) - T \circ \phi(\mathbf{x}) + J(\mathbf{x})^T \delta\mathbf{v}(\mathbf{x})\|^2$$

where $J(\mathbf{x})$ is the symmetric gradient $J(\mathbf{x}) = (\nabla R(\mathbf{x}) + \nabla(T \circ \phi)(\mathbf{x})) / 2$. It follows the linear least square problem:

$$\begin{aligned}\mathcal{P}_{corr}(\delta\mathbf{v}, p) &= \frac{1}{\sigma_i^2} \int_{\Omega} \|R(\mathbf{x}) - T \circ \phi(\mathbf{x}) + J(\mathbf{x})^T \delta\mathbf{v}(\mathbf{x})\|^2 d\mathbf{x} \\ &\quad + \frac{1}{\sigma_x^2} \int_{\Omega} \|\delta\mathbf{v}(\mathbf{x})\|^2 d\mathbf{x} - 2 \int_{\Omega} p(\mathbf{x}) \nabla \cdot \delta\mathbf{v}(\mathbf{x}) d\mathbf{x}\end{aligned}$$

The optimal condition $\partial_{\delta\mathbf{v}} \mathcal{P}_{corr}(\delta\mathbf{v}, p) = 0$ thus writes:

$$\underbrace{\left(J(\mathbf{x})J(\mathbf{x})^T + \frac{\sigma_i^2}{\sigma_x^2} \text{Id} \right)}_{D(\mathbf{x})} \delta\mathbf{v}(\mathbf{x}) = -J(\mathbf{x}) \left(R(\mathbf{x}) - T \circ \phi(\mathbf{x}) \right) - \sigma_i^2 \nabla p(\mathbf{x})$$

As the tensor $D(\mathbf{x})$ is always invertible, we can calculate the optimal divergence-free update velocity field:

$$\delta\mathbf{v}(\mathbf{x}) = -\underbrace{\left(R(\mathbf{x}) - T \circ \phi(\mathbf{x}) \right) D(\mathbf{x})^{-1} J(\mathbf{x}) - \sigma_i^2 D(\mathbf{x})^{-1} \nabla p(\mathbf{x})}_{\delta\mathbf{v}(\mathbf{x})} \quad (17)$$

The first term of the previous equation is exactly the logDemons update velocity field $\delta\mathbf{v}$ (3). The pressure field p is calculated by solving the Poisson equation under 0-Dirichlet boundary conditions that results from the divergence of the previous equation:

$$\nabla \cdot (\sigma_i^2 D(\mathbf{x})^{-1} \nabla p(\mathbf{x})) = \nabla \cdot \delta\mathbf{v}(\mathbf{x}) \quad (18)$$

Because the tensor $D(\mathbf{x})$ is updated at each iteration, the operator $\nabla \cdot (\sigma_i^2 D^{-1} \nabla)$ is not constant. The matrix of the related linear system must therefore be built and pre-conditioned at each time step, which can be computationally demanding if the domain Ω is large. Furthermore, $D(\mathbf{x})$ is computed at every voxel of the image domain Ω independently. The resulting tensor field can therefore be noisy, likely yielding numerical instabilities. To alleviate this limitation, D is smoothed using Log-Euclidian techniques (Arsigny et al, 2006b): each component of $\log(D)$ is smoothed with a Gaussian kernel G_{σ_D} and the result is exponentiated to get a smooth tensor field. In this paper, we fixed σ_D^2 equal to the strength σ_f^2 of the fluid regularisation.

D Robustness of iLogDemons with Respect to Slice Thickness

During our experiments we also quantified the robustness of the iLogDemons with respect to image slice thickness on synthetic data. The reference and the warped images of the whirl data sets were degraded by artificially increasing the slice thickness along the z-axis. Every N consecutive slices were grouped together and averaged to simulate partial volume effect. In-plane resolution was preserved. The resulting images were resampled to get 1 mm^3 -isotropic voxels. Four datasets were

generated with slice thicknesses spanning from 1 mm to 10 mm . The registration parameters were $\sigma_f^2 = 1$, $\sigma^2 = 1$ and $\sigma_x = 1$. Results are reported in Fig. 15.

Not surprisingly, increasing the slice thickness decreased the overall registration accuracy as less image information was available: RMSE and DTF steadily increased. LogDemons yielded better image matching (lower RMSE) but the recovered deformation fields were less accurate than those estimated using iLogDemons (higher DTF). Incompressibility constraints helped the algorithm to recover the incompressible whirl. This experiment also confirmed that $i^2\text{LogDemons}$ did not improve registration accuracy with respect to iLogDemons. Fig. 16 illustrates these findings on a particular case. Far from image gradients, the deformation estimated by logDemons were weak and erroneous (arrow A). Even worse, near strong image gradients, the deformation field can be completely wrong (arrow B). Thanks to the incompressibility constraint, iLogDemons alleviated these pitfalls and recovered a plausible through-plane motion (arrow C). These results motivate the use of iLogDemons to estimate the motion of incompressible organs in medical images.

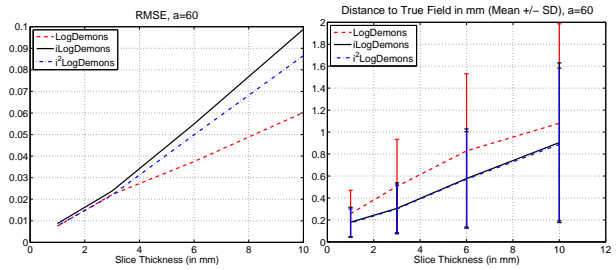


Fig. 15 RMSE and DTF with respect to slice thickness. Despite higher RMSE, estimated deformation fields are systematically more accurate using incompressible constraints (iLogDemons) than using logDemons. One can also see that constraining the update velocity to be divergence-free ($i^2\text{LogDemons}$) did not improve the results in terms of DTF. Same conclusions for all the other whirl angles.

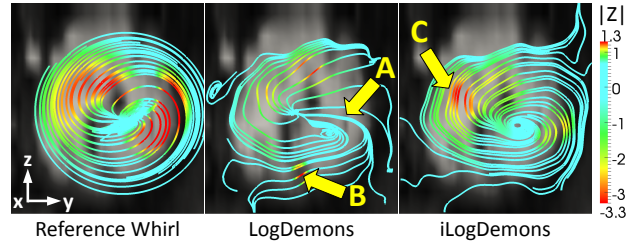


Fig. 16 Streamlines of 3D whirl transformations ($\alpha_0 = 60^\circ$) recovered from an image with 6mm-thick slices. Contrary to logDemons, which failed to recover the whirl transformation in homogeneous regions (A) and was misguided by strong gradients (B), iLogDemons improved the recovery of the through-plane whirl deformations (C) despite the lack of image information. Colours encode the amplitude of the through-plane z-direction in mm.

References

- Arnold V (1989) Mathematical methods of classical mechanics. Springer-Verlag

- Arsigny V, Commowick O, Pennec X, Ayache N (2006a) A log-euclidean framework for statistics on diffeomorphisms. In: Medical Image Computing and Computer-Assisted Intervention MICCAI, Springer, vol 4190, p 924
- Arsigny V, Fillard P, Pennec X, Ayache N (2006b) Log-Euclidean metrics for fast and simple calculus on diffusion tensors. Magnetic Resonance in Medicine 56(2):411–421
- Ashburner J, Hutton C, Frackowiak R, Johnsrude I, Price C, Friston K (1998) Identifying global anatomical differences: deformation-based morphometry. Human Brain Mapping 6(5-6):348–357
- Beg M, Miller M, Trouvé A, Younes L (2005) Computing Large Deformation Metric Mappings via Geodesic Flows of Diffeomorphisms. International Journal of Computer Vision 61(2):139–157
- Bistogram A, Oshinski J, Skrinjar O (2008) Myocardial deformation recovery from cine MRI using a nearly incompressible biventricular model. Medical Image Analysis 12(1):69–85
- Bossa M, Hernandez M, Olmos S (2007) Contributions to 3d diffeomorphic atlas estimation: application to brain images. In: Medical image computing and computer-assisted intervention: MICCAI... International Conference on Medical Image Computing and Computer-Assisted Intervention, vol 10, p 667
- Broit C (1981) Optimal registration of deformed images. PhD thesis, University of Pennsylvania
- Cachier P, Ayache N (2004) Isotropic energies, filters and splines for vectorial regularization. J of Math Imaging and Vision 20(3):251–265
- Cachier P, Pennec X, Ayache N (1999) Fast Non Rigid Matching by Gradient Descent: Study and Improvements of the "Demons" Algorithm. 0 RR-3706, INRIA, URL <http://hal.inria.fr/inria-00072962/PDF/RR-3706.pdf>
- Cachier P, Bardinet E, Dormont D, Pennec X, Ayache N (2003) Iconic feature based nonrigid registration: the PASHA algorithm. Computer Vision and Image Understanding 89(2-3):272–298
- Cahill ND, Noble JA, Hawkes DJ (2009) A demons algorithm for image registration with locally adaptive regularization. In: Yang GZ, Hawkes D, Rueckert D, Noble A, Taylor C (eds) Medical Image Computing and Computer-Assisted Intervention – MICCAI 2009, Springer, Lecture Notes in Computer Science, vol 5761, pp 574–581
- Clatz O, Delingette H, Talos I, Golby A, Kikinis R, Jolesz F, Ayache N, Warfield S, INRIA F (2005) Robust nonrigid registration to capture brain shift from intraoperative mri. IEEE transactions on medical imaging 24(11):1417–1427
- Cuzol A, Hellier P, Mémin E (2007) A low dimensional fluid motion estimator. International Journal of Computer Vision 75(3):329–349
- DeCraene M, Camara O, Bijnens B, Frangi A (2009) Large diffeomorphic ffd registration for motion and strain quantification from 3d-us sequences. In: Functional Imaging and Modeling of the Heart: 5th International Conference, Fimh 2009 Nice, France, June 3-5, 2009 Proceedings, Springer-Verlag New York Inc, p 437
- Deriche R (1993) Recursively implementing the gaussian and its derivatives. Rapports de recherche- INRIA
- Do Carmo M, Flaherty F (1992) Riemannian geometry. Birkhauser
- Dru F, Vercauteren T (2009) An ITK implementation of the symmetric log-domain diffeomorphic demons algorithm. Insight Journal – 2009 January - June, URL <http://hdl.handle.net/10380/3060>
- Evans LC (1998) Partial Differential Equations. American Mathematical Society
- Ferrant M, Nabavi A, Macq B, Jolesz F, Kikinis R, Warfield S (2001) Registration of 3d intraoperative mr images of the brain using a finite element biomechanical model. IEEE Transactions on Medical Imaging 20(12):1384–1397
- Glass L, Hunter P, McCulloch A (1991) Theory of Heart: Biomechanics, Biophysics, and Nonlinear Dynamics of Cardiac Function. Springer-Verlag
- Glockner H (2006) Fundamental problems in the theory of infinite-dimensional lie groups. Arxiv preprint math/0602078
- Gorce J, Fribolet D, Magnin I (1997) Estimation of three-dimensional cardiac velocity fields: assessment of a differential method and application to three-dimensional CT data. Medical Image Analysis 1(3):245–261
- Haber E, Modersitzki J (2004) Numerical methods for volume preserving image registration. Inverse Problems 20(5):1621–1638
- Heitz D, Mémin E, Schnörr C (2009) Variational fluid flow measurements from image sequences: synopsis and perspectives. Experiments in Fluids pp 1–25
- Hernandez M, Bossa M, Olmos S (2009) Registration of anatomical images using paths of diffeomorphisms parameterized with stationary vector field flows. International Journal of Computer Vision 85(3):291–306
- Hinkle J, Fletcher P, Wang B, Salter B, Joshi S (2009) 4d map image reconstruction incorporating organ motion. In: Proceedings of the 21st International Conference on Information Processing in Medical Imaging, Springer, p 687
- Horn B, Schunck B (1981) Determining optical flow. Artificial intelligence 17(1-3):185–203
- Mansi T, Peyrat JM, Sermesant M, Delingette H, Blanc J, Boudjemline Y, Ayache N (2009) Physically-constrained diffeomorphic demons for the estimation of 3d myocardium strain from cine-mri. In: Proceedings of Functional Imaging and Modeling of the Heart 2009 (FIMH'09), LNCS, vol 5528, pp 201–210
- Martin Bland J, Altman D (1986) Statistical methods for assessing agreement between two methods of clinical measurement. The Lancet 327(8476):307–310
- Miller MI, Trouvé A, Younes L (2002) On the metrics and Euler-Lagrange equations of computational anatomy. Annual Review of Biomed Eng 4:375–405
- Modersitzki J (2004) Numerical Methods for Image Registration. Oxford University Press
- Moore C, Lugo-Olivieri C, McVeigh E, Zerhouni E (2000) Three-dimensional systolic strain patterns in the normal human left ventricle: Characterization with tagged MR imaging. Radiology 214(2):453–466
- Nielsen M, Florack L, Deriche R (1994) Regularization and scale space e. Tech. rep., INRIA: Institut National de Recherche en Informatique et en Automatique
- Papademetris X, Sinusas A, Dione D, Constable R, Duncan J (2000) Estimating 3D strain from 4D cine-MRI and echocardiography: In-vivo validation. In: MICCAI 2000, Springer, pp 678–686
- Pennec X, Cachier P, Ayache N (1999) Understanding the "demon's algorithm": 3D non-rigid registration by gradient descent. In: Taylor C, Colchester A (eds) Proc. of 2nd Int. Conf. on Medical Image Computing and Computer-Assisted Intervention (MICCAI'99), Springer, Cambridge, UK, LNCS, vol 1679, pp 597–605
- Phatak N, Maas S, Veress A, Pack N, Di Bella E, Weiss J (2009) Strain measurement in the left ventricle during systole with deformable image registration. Medical Image Analysis 13:354–361
- Rohlfing T, Maurer Jr C, Bluemke D, Jacobs M (2003) Volume-preserving nonrigid registration of MR breast images using free-form deformation with an incompressibility constraint. Medical Imaging, IEEE Transactions on 22(6):730–741
- Rueckert D, Sonoda L, Hayes C, Hill D, Leach M, Hawkes D (1999) Nonrigid registration using free-form deformations: application to breast MR images. IEEE Transactions on Medical Imaging 18(8):712–721
- Rueckert D, Aljabar P, Heckemann R, Hajnal J, Hammers A (2006) Diffeomorphic registration using b-splines. In: Medical image computing and computer-assisted intervention: MICCAI... International Conference on Medical Image Computing and Computer-Assisted Intervention, vol 9, p 702

-
- Saddi KA, Chefd'hotel C, Cheriet F (2007) Large deformation registration of contrast-enhanced images with volume-preserving constraint. In: Proceedings of SPIE Medical Imaging, SPIE, vol 6512
- Simard PY, Mailloux GE (1988) A projection operator for the restoration of divergence-free vector fields. *IEEE Transactions on Pattern Analysis and Machine Intelligence* 10(2):248–256
- Sinusas A, Papademetris X, Constable R, Dione D, Slade M, Shi P, Duncan J (2001) Quantification of 3-D regional myocardial deformation: shape-based analysis of magnetic resonance images. *American Journal of Physiology- Heart and Circulatory Physiology* 281(2):698–714
- Song S, Leahy R (1991) Computation of 3-D velocity fields from 3-D cine CT images of a human heart. *IEEE Transactions on Medical Imaging* 10(3):295–306
- Sorzano C, Thévenaz P, Unser M (2005) Elastic registration of biological images using vector-spline regularization. *IEEE Transactions on Biomedical Engineering* 52(4):652–663
- Sundar H, Davatzikos C, Biros G (2009a) Biomechanically-constrained 4d estimation of myocardial motion. In: Yang GZ, Hawkes D, Rueckert D, Noble A, Taylor C (eds) *Medical Image Computing and Computer-Assisted Intervention – MICCAI 2009*, Springer, Lecture Notes in Computer Science, vol 5762, pp 257–265
- Sundar H, Littb H, Shena D (2009b) Estimating myocardial motion by 4d image warping. *Pattern Recognition* 42:2514–2526
- Thirion JP (1998) Image matching as a diffusion process: an analogy with Maxwell's demons. *Medical Image Analysis* pp 243–260
- Vercauteren T, Pennec X, Perchant A, Ayache N (2008) Symmetric log-domain diffeomorphic registration: A demons-based approach. In: Metaxas D, Axel L, Fichtinger G, Székely G (eds) *Proc. Medical Image Computing and Computer Assisted Intervention (MICCAI'08)*, Part I, Springer-Verlag, New York, USA, Lecture Notes in Computer Science, vol 5241, pp 754–761
- Vercauteren T, Pennec X, Perchant A, Ayache N (2009) Diffeomorphic demons: Efficient non-parametric image registration. *NeuroImage* 45(1S1):61–72
- Veress A, Gullberg G, Weiss J (2005) Measurement of Strain in the Left Ventricle during Diastole with cine-MRI and Deformable Image Registration. *Journal of Biomechanical Engineering* 127:1195